ORGANOMETALLICS

pubs.acs.org/Organometallics Article

Pitfalls for POCOP-Type Palladium Pincer Complexes in Catalytic Reduction of CO_2 with Catecholborane

Anubendu Adhikary,* Sayantani Saha, N. Sai Kumar, Allen G. Oliver, Jeanette A. Krause, and Hairong Guan*

Cite This: *Organometallics* 2023, 42, 1525−1537 Read Online

ACCESS | Metrics & More | Article Recommendations | Supporting Information

ABSTRACT: Reduction of CO_2 with catecholborane (HBcat) is known to be catalyzed by nickel hydride complexes supported by a bis(phosphinite)-based or POCOP-type pincer ligand. The objective of this research is to examine how changing the metal center from nickel to palladium would impact the outcome of CO_2 reduction. Stoichiometric studies show that the palladium hydride complexes react rapidly with CO_2, although the resulting palladium formate complexes can lose CO_2 under reduced pressure or in chloroform. In the presence of HBcat, the formate complexes are converted back to the palladium hydride species while the formate group is reduced to CH_3OBcat. This process is also accompanied by the formation of palladium bis(catecholato)borate complexes, which diverts some of the HBcat to yield $B_2(cat)_3$ and B_2H_6. For palladium hydrides stabilized by a POCOP-pincer ligand with relatively small phosphorus substituents (e.g., isopropyl or cyclopentyl groups), HBcat cleaves the P−O bonds in the ligand backbone to degrade the catalysts to secondary phosphine complexes. Without CO_2, HBcat also undergoes H_2 elimination with the Pd−H moiety to form palladium boryl complexes. These side reactions with HBcat and the palladium pincer complexes play profound roles in the catalytic reduction of CO_2 with the borane.

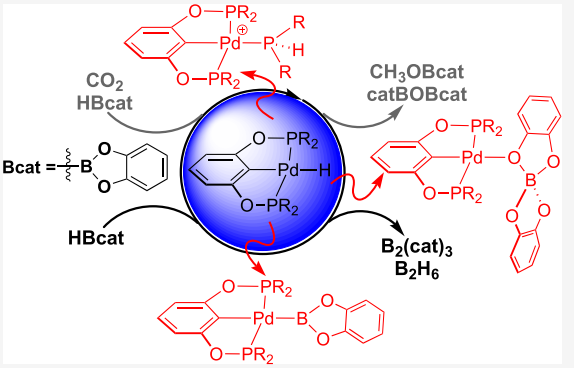

INTRODUCTION

Reduction of CO_2 to fuels or fine chemicals has been a subject of extensive study for decades, pursued by many researchers across different fields of catalysis.[1] These efforts have led to the development of a myriad of strategies for CO_2 transformation under reducing conditions, which are typically classified into thermochemical,[2,3] photochemical,[4] and electrochemical approaches.[4a−c,5] Ideally, the catalytic reduction of CO_2 should be performed in conjunction with light harvesting or, alternatively, through the use of photogenerated H_2. In this context, employing main-group hydrides such as silanes and boranes to reduce CO_2 is unlikely to provide the best solution for energy storage or CO_2 utilization, unless the hydrides can be inexpensively regenerated from H_2. However, an in-depth mechanistic understanding of the reduction processes can provide useful guidelines for designing more effective strategies to convert CO_2 and solar energy to fuels or value-added chemicals. In addition, with main-group hydrides, it is possible to selectively convert CO_2 to valuable C_1 building blocks (e.g., $X_2BOCH_2OBX_2$) that are otherwise difficult to access.[6]

Borohydrides, including the ones as simple as $NaBH_4$, can react directly with CO_2 to give formatoborates ($[HCO_2BX_3]^-$),[7,8] although using a catalyst allows CO_2 to be further reduced to the methoxide level ($[CH_3OBX_3]^-$).[9,10] Boranes such as BH_3·THF, catecholborane (HBcat), pinacolborane (HBpin), and 9-borabicyclo[3.3.1]nonane (9-BBN) are less hydridic than anionic borohydrides;[11] if used for CO_2 reduction, a catalyst would be needed. In these hydroboration processes,[12] the catalyst plays the role of enhancing the hydricity of the B−H moiety, increasing the electrophilicity of the carbonyl groups, and/or providing a hydride shuttle from boron to CO_2 as well as the transient products. To date, a plethora of molecular catalysts have been developed to promote the reduction of CO_2 with boranes, ranging from Lewis bases (amines,[13] phosphines,[14] and carbon-based nucleophiles[15]) and frustrated Lewis pairs[13a,16] to main-group hydrides ([B]−H,[7a,8c−f,17] [Al]−H,[17c,18] [Ga]−H,[19] [Ge]−H,[20] and [Sn]−H[20]) and metal complexes (containing Mo,[21] Mn,[22] Fe,[6b,23] Ru,[6a,24] Co,[23,25] Ir,[26] Ni,[6c,27] Pd,[6c,27h,28] Cu,[23,29] or Zn[30]).

We have contributed to this research area with the reports of diphosphinite-derived or POCOP-pincer-type nickel hydride complexes as catalysts for the reduction of CO_2 with boranes

Received: March 7, 2023
Published: May 18, 2023

Scheme 1. Key Steps in the Hydroboration of CO_2 Catalyzed by a POCOP-Pincer-Ligated Nickel Hydride Complex

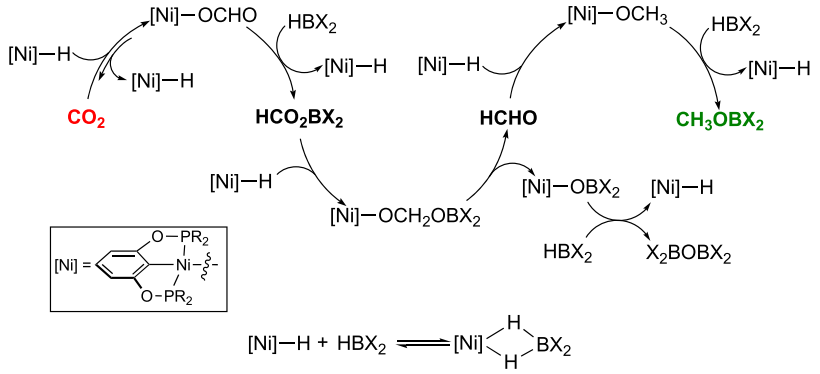

Chart 1. Nickel and Palladium Pincer Complexes Studied as Catalysts or Precatalysts for the Hydroboration of CO_2

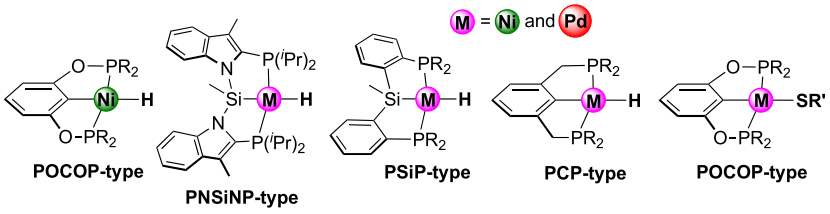

(HBX_2 = HBcat, 9-BBN).[27a−d,g] The catalytic reactions operate under relatively mild conditions (room temperature, p_{CO_2} = 1 atm), resulting in the selective reduction of CO_2 to CH_3OBX_2. On the basis of nuclear magnetic resonance (NMR) studies and density functional theory (DFT) calculations, we have proposed a mechanism (Scheme 1) involving three consecutive, formally two-electron reduction processes to complete the reaction sequence of CO_2 → HCO_2BX_2 → HCHO → CH_3OBX_2.[27b,d] The metal complex, in essence, shuttles the hydride from HBX_2 to CO_2, HCO_2BX_2, and HCHO via carbonyl insertion into the nickel−hydrogen bond. We have also found that, depending on the Lewis acidity of HBX_2, [Ni]−H may partially or fully engage in the interaction with HBX_2 to form a κ^2-H_2BX_2 complex, which reduces the steady-state concentration of the catalytically active hydride species.[27d] While absent in our catalytic system, the interception of [Ni]−OCH_2OBX_2 by HBX_2 to form $X_2BOCH_2OBX_2$ can be a competing pathway, as demonstrated by the Turculet group in their study of PNSiNP-type nickel and palladium hydride complexes (see Chart 1) for the catalytic reduction of CO_2 with HBpin.[6c] A more detailed investigation by Hazari and co-workers focusing on PSiP- and PCP-type pincer complexes has shown that the selectivity for HCO_2BX_2, $X_2BOCH_2OBX_2$, or CH_3OBX_2 can be judiciously tuned by varying the metal center, pincer ligand, borane, and concentration, or adding $B(OPh)_3$ as a cocatalyst.[27h] The catalytic systems that more closely resemble ours are those developed by Zhang, Chen, and co-workers, featuring nickel and palladium *thiolate* complexes supported by a POCOP-pincer ligand.[27f,28b] Given the structural similarity, one might have anticipated that, in the presence of HBX_2, these thiolate complexes would be converted to the hydride species, thus converging into the mechanistic steps shown in Scheme 1. The thiolate-catalyzed reactions are, however, more efficient, and display more complicated NMR spectra than the reactions that directly employ the hydride complexes as the catalysts. According to DFT calculations of a nickel catalyst with HBcat,[31] the nickel thiolate system produces a [Ni]−$O(BH_3)(C_6H_4OBcat)$ complex, which is presumably more reactive than the corresponding nickel hydride complex.

The advantage of using HBcat to reduce CO_2 is that the selectivity often favors the more reduced product, namely, CH_3OBcat, possibly because HBcat has a small steric profile with a more electropositive boron center.[27h,32] It is interesting to note that, for the PSiP- and PCP-pincer systems, palladium hydrides outperform their nickel analogs with respect to CH_3OBcat yield.[27h] In contrast, a computational study of the truncated PCP-pincer molecules suggests that CO_2 insertion is more favorable with nickel hydrides, both kinetically and thermodynamically.[33,34] It is likely that the overall catalytic activity is not solely determined by the insertion steps. Comparison of nickel and palladium thiolate complexes for the catalytic reduction of CO_2 with HBcat is even less straightforward; the periodic trend for the catalytic activity changes when the phosphorus substituent or the SR' group is altered.[27f,28b] To provide the missing link in the POCOP-pincer series and to further understand the differences between nickel and palladium systems, we present here a catalytic study of the palladium hydride complexes for CO_2 reduction with HBcat. This research was also motivated by the fact that the palladium hydrides have weaker interactions with boranes than the nickel hydrides,[35] which should be beneficial for the productive steps that require free hydride species.

RESULTS AND DISCUSSION

CO_2 Insertion into the Palladium Hydrides. To establish the insertion chemistry, the POCOP-pincer-ligated palladium hydride complexes {2,6-$(R_2PO)_2C_6H_3$}PdH (**1a−c**)[36,37] were mixed with CO_2 (1 atm) in C_6D_6 (Scheme 2), which resulted in the rapid and quantitative formation of {2,6-$(R_2PO)_2C_6H_3$}PdOCHO (**2a−c**). The most notable spectroscopic change was the disappearance of the hydride resonance (**1a**: δ −2.48; **1b**: δ −2.40; **1c**: δ −2.37) and the emergence of a formate resonance in the downfield region (**2a**: δ 8.93; **2b**: δ 8.76; **2c**: δ 8.77). This facile insertion of CO_2 is analogous to the reactivity previously reported for palladium hydride

https://doi.org/10.1021/acs.organomet.3c00126
Organometallics 2023, 42, 1525−1537

Scheme 2. Palladium Formate Complexes Generated via Insertion of CO_2 or Protonation with HCO_2H

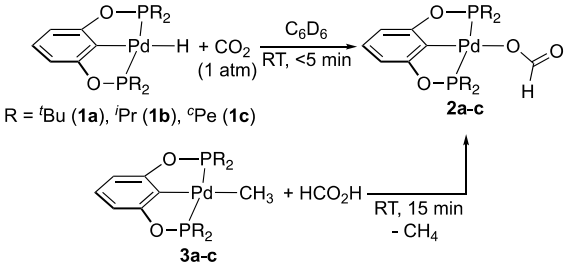

complexes supported by a PCP- or PSiP-pincer ligand.[33,38] The formate complexes were alternatively synthesized from the palladium methyl complexes (**3a–c**) via protonation with HCO_2H.

Isolation of **2a–c** in the solid form is feasible; however, the samples should not be kept under vacuum longer than necessary because decarboxylation will occur. In contrast, the analogous POCOP-type nickel formate complexes can survive prolonged evacuation without losing CO_2, suggesting that the kinetic barriers for decarboxylation are higher with nickel. Compounds **2b** and **2c** are readily soluble in benzene and toluene, whereas **2a** has limited solubility in these solvents. To obtain a $^{13}C\{^1H\}$ NMR spectrum with a reasonable signal-to-noise ratio, **2a** was dissolved in $CDCl_3$ for a rapid NMR analysis. The same sample left standing for 48 h showed a quantitative conversion of **2a** to the corresponding palladium chloride complex (**4a**) along with $CHDCl_2$ (δ_H 5.28) and CO_2 (δ_C 125.0) (eq 1). This result further supports that CO_2 insertion is reversible.[39]

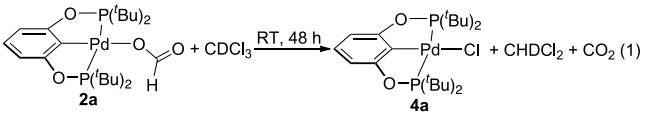

The solid-state structures of **2a** and **2b** were determined by X-ray crystallography. As illustrated in Figure 1, the Pd atom in **2a** is situated in a distorted square-planar environment with the O3 atom displaced 0.40 Å out of the least-square plane defined by the P1, C1, P2, and Pd atoms. The formate group adopts a conformation that is nearly perpendicular to the coordination plane; the dihedral angle between P1–C1–P2–Pd and O3–C23–O4 planes is 74.7°. In contrast, the formate group in **2b** rotates only slightly out of the coordination plane (Figure 2), giving a dihedral angle of 14.4°. The perpendicular conformation is more frequently encountered in pincer-supported nickel and palladium formate complexes,[27a,33,40] although for {2,6-(^{i}Pr$_2$PO)$_2$C$_6$H$_3$}NiOCHO (**5b**) and {2,6-(^{c}Pe$_2$PO)$_2$C$_6$H$_3$}NiOCHO (**5c**), the "in-plane" conformation has also been observed for the formate group.[27c] Nevertheless, in solution, the Pd–O3 bond rotation does not appear to be restricted, as judged by the limited number of NMR resonances.

Catalytic Reduction of CO_2 with HBcat. Having established that the palladium hydrides can stoichiometrically reduce CO_2, we proceeded to investigate the catalytic reactions using HBcat as the hydride source. The formate complexes **2a–c** were chosen as the entry point into the catalytic cycles because they are less air sensitive than their hydride derivatives. In our previous study of the nickel POCOP-pincer system,[27a,c,d] HBcat was always added before the CO_2 gas was introduced. In this work, the same procedure was adopted,

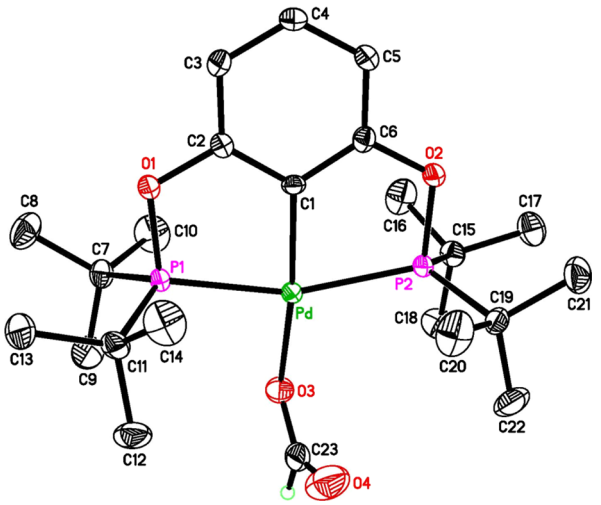

Figure 1. Oak Ridge Thermal Ellipsoid Plot (ORTEP) of {2,6-(^{t}Bu$_2$PO)$_2$C$_6$H$_3$}PdOCHO (**2a**) at 50% probability level (all hydrogen atoms except for the formate group are omitted for clarity). Selected interatomic distances (Å) and angles (deg): Pd–C1 1.990(2), Pd–O3 2.1056(19), Pd–P1 2.2903(6), Pd–P2 2.3088(6), C23–O3 1.259(4), C23–O4 1.220(4); P1–Pd–P2 160.29(2), C1–Pd–O3 169.60(9), C1–Pd–P1 80.22(7), C1–Pd–P2 80.16(7), O3–Pd–P1 96.04(6), O3–Pd–P2 103.61(6).

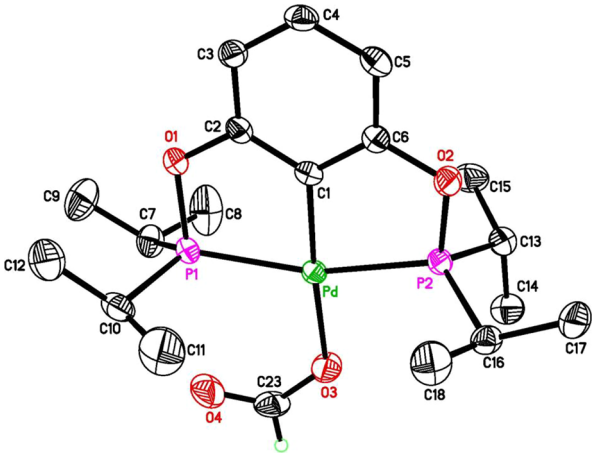

Figure 2. ORTEP of {2,6-(^{i}Pr$_2$PO)$_2$C$_6$H$_3$}PdOCHO (**2b**) at 50% probability level (all hydrogen atoms except for the formate group are omitted for clarity). Selected interatomic distances (Å) and angles (deg): Pd–C1 1.977(2), Pd–O3 2.0986(18), Pd–P1 2.2927(6), Pd–P2 2.2778(6), C23–O3 1.267(4), C23–O4 1.236(4); P1–Pd–P2 160.79(2), C1–Pd–O3 176.15(9), C1–Pd–P1 80.79(7), C1–Pd–P2 80.34(7), O3–Pd–P1 102.67(6), O3–Pd–P2 96.30(6).

and for selected experiments the addition order was reversed in an effort to understand if such a modification would change the reaction outcome. For comparison purposes, catalytic activities of the nickel formate complexes {2,6-(R_2PO)$_2$C$_6$H$_3$}NiOCHO (**5a–c**) were also examined. These catalytic results are all summarized in Table 1.

Following the HBcat-first procedure, the reaction catalyzed by **2a** (1 mol % with respect to HBcat) converted CO_2 to CH_3OBcat with a turnover number (TON) of 85 obtained in 1 h (entry 1). When the reaction time was extended to 4 h, the amount of CH_3OBcat did not increase, suggesting that the reduction process had ceased. Reversing the addition order had minimal impact on the TONs measured at 1 and 4 h (entry 2).

https://doi.org/10.1021/acs.organomet.3c00126
Organometallics 2023, 42, 1525–1537

Table 1. Palladium- and Nickel-Catalyzed Reduction of CO_2 with HBcat[a]

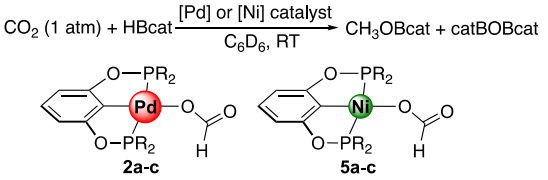

entry	catalyst	addition order	TON_{1h}[b]	TON_{4h}[b]	TON_{12h}[b]
1	**2a**	HBcat first	85	85	
2	**2a**	CO_2 first	82	89	
3	**2b**	HBcat first	85	84	
4	**2b**	CO_2 first	82	81	
5	**2c**	CO_2 first	92	89	
6	**5a**	HBcat first	100		
7	**5b**	HBcat first		100	
8	**5b**	CO_2 first		97	
9	**5c**	HBcat first			30
10	**5c**	CO_2 first	84		

[a]Reaction conditions: catalyst (25 μmol), HBcat (2.5 mmol), and hexamethyldisilane (50 μmol, internal standard) in 2.0 mL of C_6D_6 at room temperature (23 °C) under 1 atm of CO_2. [b]Based on the B−H bond that participates in the reduction of CO_2.

Interestingly, for the less bulky catalysts, **2b** gave almost the same results (entries 3 and 4) and **2c** performed marginally better (entry 5). The analogous nickel formate complexes had a markedly different behavior, as follows: (1) the maximum TON of 100 was achievable with both **5a** and **5b** (entries 6 and 7); (2) the catalytic reaction was more efficient when the sterically more demanding catalyst **5a** was employed (entry 6 vs entries 7 and 9); and (3) the addition order mattered in the case of **5c**, where the CO_2-first procedure gave a higher TON (entry 10 vs entry 9). The differences noted here for the palladium and nickel catalysts do not necessarily suggest that the palladium system does not proceed via the mechanistic steps as outlined in Scheme 1. Instead, other competing pathways may be involved, which became the next focus of our study.

Reactions of the Palladium Formate Complexes with HBcat. The failure to achieve the maximum TON with the palladium catalysts hinted to us that, in addition to reducing CO_2, HBcat might also participate in some unproductive reactions. To further probe the details, the stoichiometric reactions between the formate complexes **2a−c** and HBcat were investigated. In each experiment, 3 equiv of HBcat was added, which according to Scheme 1 is the amount needed to fully convert a formate complex to CH_3OBcat.

Complex **2a** was first suspended in C_6D_6, which became a clear solution upon mixing with HBcat. The ^1H and ^{11}B NMR spectra recorded at 15 min showed the expected product CH_3OBcat (along with catBOBcat); however, its NMR yield was only 87%. Other potentially formed products such as HCO_2Bcat, $catBOCH_2OBcat$, and HCHO were not detected. Extending the reaction time did not further increase the yield of CH_3OBcat, confirming that reduction of the formate group was already complete. In contrast, a similar reaction between the nickel formate complex **5a** and HBcat yielded CH_3OBcat quantitatively. The $^{31}P\{^1H\}$ NMR spectra shed more light on why a lesser amount of CH_3OBcat was obtained from the palladium system. Evidently, HBcat reacted with **2a** to form three pincer complexes (eq 2) with phosphorus resonances observed at δ 213.8 (76%), 192.3 (5%), and 192.2 (19%). This composition did not change over a period of 12 h. The major species can be identified as the palladium hydride **1a**.[36] The resonance at δ 192.3 (**7a**) remains unknown at the moment,[41] while the resonance at δ 192.2 is attributed to a palladium bis(catecholato)borate complex (**6a**), which will be discussed in the next section. It is worth mentioning that under the same conditions the nickel formate complex **5a** was converted to the corresponding nickel hydride without forming additional pincer complexes.

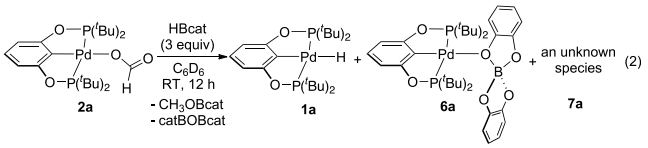

The reaction of HBcat with a sterically less bulky formate complex, **2b** or **2c**, is much more complicated. In addition to the expected hydride complex, more than four palladium species were observed at the beginning of the reaction (<15 min). Nevertheless, the NMR spectra recorded after 12 h are more interpretable. In the case of **2b**, the initially formed palladium hydride **1b** disappeared completely, and the main palladium species (δ 186.8, 91% of all pincer complexes) became the bis(catecholato)borate complex **6b** (eq 3). The identity of a minor species (**7b**, δ 187.9, 4%) remains unknown. The third palladium species (5%) has characteristic phosphorus resonances at δ 197.3 (doublet, J_{P-P} = 32.4 Hz) and δ 4.1 (triplet, J_{P-P} = 32.4 Hz), which integrate to a 2:1 ratio. The chemical shift values and the splitting pattern are reminiscent of our previously reported compounds that originated from degradation of the pincer framework.[27d,36,42] We thus suspected that this species could be a pincer complex bearing a secondary phosphine ([**8b**]BH_4), which was generated via cleavage of the P−O bonds by HBcat. The counterion BH_4^- is assigned here based on the observed ^{11}B NMR resonance at δ −39.7.[43] The reaction of HBcat with **2c** was similar, producing a mixture of **6c** (δ 179.5, 74%), [**8c**]BH_4 (δ 186.3 and −1.8, J_{P-P} = 32.4 Hz, 20%), and an unknown palladium species (**7c**, δ 179.7, 6%) after 12 h. In both cases, the NMR yield for CH_3OBcat was not quantitative (~85%), consistent with the fact that forming byproducts **6b**/**6c** and [**8b**]BH_4/[**8c**]BH_4 sacrifices some HBcat. In our previous study of the nickel system,[27c] {2,6-($^cPe_2PO$)$_2C_6H_3$}-NiOCHO (**5c**) was also shown to undergo pincer degradation while reacting with HBcat at the formate site. These results seem to suggest that, without sufficient steric protection, the P−O bonds are vulnerable to attack by HBcat, regardless of the nature of the central metal.

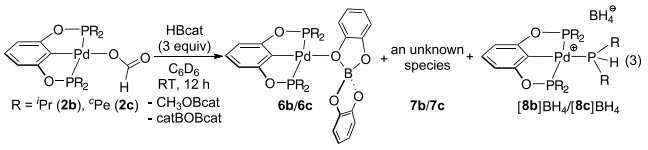

[**8b**]$^+$ and [**8c**]$^+$ with a triflate counterion were readily synthesized from the palladium chloride complexes **4b** and **4c**, respectively, following the procedures shown in eq 4. These secondary phosphine complexes were fully characterized by NMR and elemental analysis; [**8b**]OTf was further confirmed by X-ray crystallography (Figure 3). Due to counterion effects,

https://doi.org/10.1021/acs.organomet.3c00126
Organometallics 2023, 42, 1525−1537

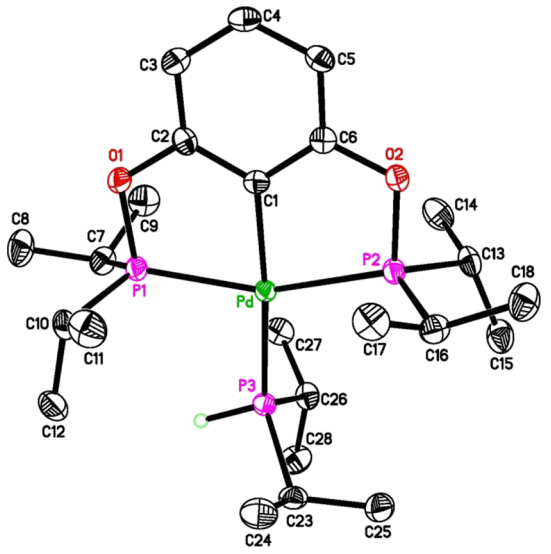

Figure 3. ORTEP of $[\{2,6\text{-}(^{i}Pr_2PO)_2C_6H_3\}Pd(HP^{i}Pr_2)]^+$ ($[\mathbf{8b}]^+$) at 50% probability level (all hydrogen atoms except the one bound to P3 are omitted for clarity). Selected interatomic distances (Å) and angles (deg): Pd−C1 2.036(2), Pd−P1 2.2967(5), Pd−P2 2.3241(5), Pd−P3 2.3723(5); P1−Pd−P2 157.40(2), P1−Pd−P3 95.789(19), P2−Pd−P3 106.66(2), C1−Pd−P1 78.92(6), C1−Pd−P2 78.91(6), C1−Pd−P3 172.94(6).

the NMR data for [**8b**]OTf and [**8c**]OTf do not match exactly with those described above but they are reasonably close. In the $^{31}P\{^{1}H\}$ NMR spectra, [**8b**]OTf (in C_6D_6) appears as a doublet at δ 197.8 and a triplet at δ 1.1 (J_{P-P} = 32.4 Hz), whereas [**8c**]OTf features a doublet at δ 186.2 and a triplet at δ −4.7 (J_{P-P} = 30.2 Hz). The P*H* resonances of [**8b**]OTf and [**8c**]OTf were located at δ 4.99 and 5.11, respectively, with a large $^{1}J_{H-P}$ coupling constant of ∼340 Hz. These resonances were also found from the reactions shown in eq 3, further supporting the proposed structures of $[\mathbf{8b}]BH_4$ and $[\mathbf{8c}]BH_4$.

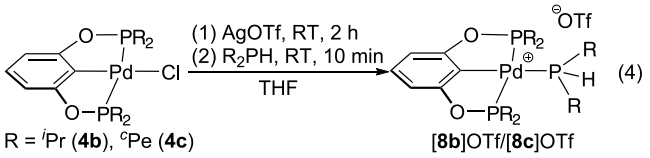

Reactions of the Palladium Hydrides with HBcat. The high affinity of boron for oxygen likely provides the driving force for HBcat to react with various Pd−O bonds formed during the reduction process. In doing so, the palladium hydride species is continuously regenerated until HBcat is depleted. With that in mind, one may interpret the side reactions in eqs 2 and 3 as an outcome from the interactions of the palladium hydrides with HBcat. Contradictory to this belief, the 1:1 mixture of the hydride complex **1a** and HBcat (in C_6D_6) showed no sign of forming the bis(catecholato)-borate complex **6a** and the unknown species **7a**, even when the mixture was kept at 50 °C for 24 h. The NMR spectra exhibited the expected signals for **1a** and HBcat except the Pd*H* and B*H* resonances had disappeared. This phenomenon is no different from what was previously observed with $\{2,6\text{-}(^{t}Bu_2PO)_2C_6H_3\}NiH$, which was rationalized by a rapid and reversible hydride exchange between the metal and boron.[27d]

In an attempt to recover **1a**, the aforementioned sample was placed under vacuum for 1 h and the residue was redissolved in C_6D_6 for NMR analysis. Interestingly, in addition to the recovered **1a** (87%), both **6a** (10%) and **7a** (3%) were also present. However, the conditions under which this mixture was produced are very different from those shown in eq 2, suggesting that the formation of **6a** and **7a** from the formate complex **2a** and HBcat is promoted by an X-type ligand other than the hydride, which could be OBcat or OCH_3.

Complex **6a** is enrichable from the mixture of **1a** and HBcat, provided a large excess of HBcat (75 equiv) is added initially and diethyl ether is used during the work-up (see Experimental Section for details). The isolated material, though contaminated with $B_2(cat)_3$,[44] showcased a phosphorus resonance at δ 192.2 as described earlier and a boron resonance at δ 14.5, consistent with a molecule bearing $[B(cat)_2]^-$.[27f,45] The structure was more unambiguously established by X-ray crystallography (Figure 4). Unlike most bis(catecholato)borate

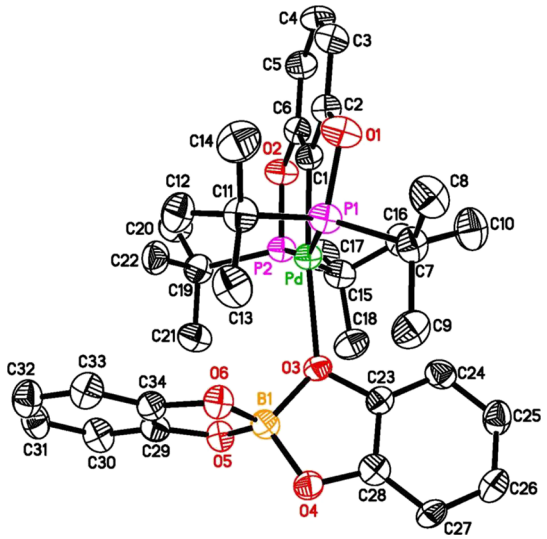

Figure 4. ORTEP of $\{2,6\text{-}(^{t}Bu_2PO)_2C_6H_3\}PdB(cat)_2$ (**6a**) at 50% probability level (cocrystallized C_6D_6 molecule and all hydrogen atoms are omitted for clarity). Selected interatomic distances (Å) and angles (deg): Pd−C1 1.990(4), Pd−P1 2.3530(12), Pd−P2 2.3384(12), Pd−O3 2.200(3), B1−O3 1.536(6), B1−O4 1.459(6), B1−O5 1.478(6), B1−O6 1.471(6); P1−Pd−P2 158.01(4), C1−Pd−O3 173.78(15), C1−Pd−P1 79.41(13), C1−Pd−P2 79.49(13), O3−B1−O4 103.6(4), O5−B1−O6 105.3(4), O3−Pd−P1 102.24(8), O3−Pd−P2 99.40(8).

complexes that use the arene π-system to coordinate to the metal,[45a,b,46] **6a** features κ^1-coordination of $[B(cat)_2]^-$ through the oxygen atom. In titanocene compounds, $[B(cat)_2]^-$ often adopts a κ^2-coordination mode using one oxygen atom from each catecholato group.[47] To our knowledge, the only reported example of a κ^1-$B(cat)_2$ transition metal complex[48] is $\{2,6\text{-}(^{t}Pr_2PO)_2C_6H_3\}NiB(cat)_2$, which was isolated following the hydroboration of CO_2 catalyzed by a nickel thiolate complex.[27f] Despite the low molecular symmetry observed in the solid state, **6a** dissolved in C_6D_6 displayed ^{13}C NMR resonances that are more consistent with a symmetrical structure (e.g., only one set of ^{t}Bu resonances and only three resonances for $[B(cat)_2]^-$). It is likely that, in solution, the palladium-bound oxygen can rapidly exchange with other oxygen atoms in $[B(cat)_2]^-$.

https://doi.org/10.1021/acs.organomet.3c00126
Organometallics 2023, 42, 1525−1537

Scheme 3. Proposed Mechanism for the Reaction of 1a with HBcat

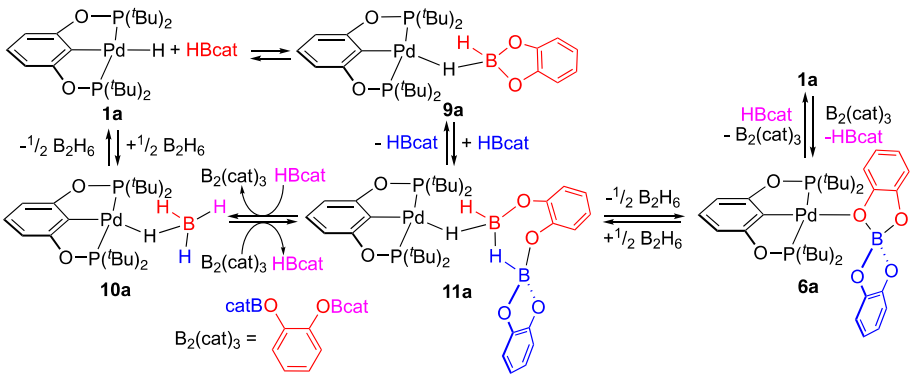

Degradation of HBcat to $[B(cat)_2]^-$, B_2H_6, and/or $B_2(cat)_3$ is known to be promoted by certain nucleophiles including metal hydrides.[44,45b,49] It has also been reported that $B_2(cat)_3$ can react with BH_3·THF to revert back to HBcat.[50] Given these precedents, we speculate that **1a** interacts with HBcat via its hydride ligand to form a κ^1-dihydridoborate complex (**9a**) as shown in Scheme 3. The proposed coordination mode is based on the closely related borohydride complex {2,6-(^{t}Bu$_2$PO)$_2$C$_6$H$_3$}PdBH$_4$ (**10a**) that has been crystallographically characterized.[35] The H−B bond formation in **9a** is expected to weaken the B−O bonds, to the extent that the attack of oxygen on the second HBcat molecule becomes possible. The resulting intermediate **11a** can further react with HBcat to yield **10a** and $B_2(cat)_3$ or, alternatively, release B_2H_6 to yield **6a**. These steps are likely reversible; increasing the HBcat/**1a** ratio, applying vacuum conditions, and adding diethyl ether during the work-up presumably shifts the equilibria to favor the formation of **6a** and $B_2(cat)_3$. Compared to **1a**, the nickel analog {2,6-(^{t}Bu$_2$PO)$_2$C$_6$H$_3$}NiH possesses a more electron-deficient metal center, as evidenced by a stronger affinity for boranes and the preference for a κ^2-coordination mode adopted by the resulting dihydridoborate.[27d] Consequently, the B−O bonds are stronger than those in **9a**, which explains why {2,6-(^{t}Bu$_2$PO)$_2$C$_6$H$_3$}NiH does not cause HBcat to degrade to $[B(cat)_2]^-$ and other boron-containing products.

As expected, replacing the *tert*-butyl groups with isopropyl groups as the phosphorus substituents makes the palladium hydride more reactive toward HBcat. According to NMR studies, adding just 1 equiv of HBcat to a solution of **1b** in C_6D_6 resulted in the consumption of the palladium hydride. The most surprising finding was the formation of H_2 (δ 4.47), implying that {2,6-(^{i}Pr$_2$PO)$_2$C$_6$H$_3$}PdBcat (**12b**) was also produced. The ^{11}B NMR spectrum indeed displayed a resonance at δ 50.3, characteristic of a metal boryl species.[51] The ^{31}P{^{1}H} NMR spectrum recorded after 15 min showed a mixture of **1b** (56%), **6b** (6%), and **12b** (38%). Extending the reaction time to 12 h allowed more **1b** to react at which point **6b** and **12b** constituted 8 and 70%, respectively, of all palladium pincer complexes (eq 5). The remaining phosphorus-containing species were identified as the unreacted hydride **1b** (6%) and the pincer degradation product [**8b**]BH$_4$ (16%). Attempts to purify **12b** were unsuccessful; however, an analytically pure sample of **6b** was obtained following recrystallization of the crude products in benzene. Like **6a**, in the solid state, **6b** bears a κ^1-B(cat)$_2$ ligand to complete the coordination sphere for a square-planar Pd(II) center (Figure 5); in solution, the coordination of $[B(cat)_2]^-$ is likely fluxional, making the structure more symmetrical. The Pd−O and Pd−P bonds in **6b** are ∼0.04 Å shorter than those in **6a**, reflecting a less sterically demanding POCOP-pincer ligand.

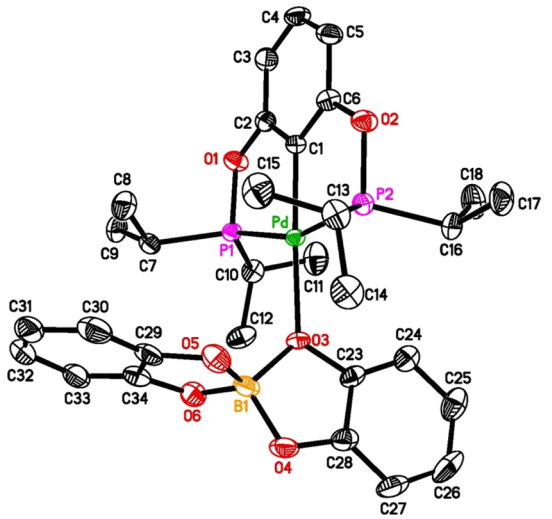

Figure 5. ORTEP of {2,6-(^{i}Pr$_2$PO)$_2$C$_6$H$_3$}PdB(cat)$_2$ (**6b**) at 50% probability level (all hydrogen atoms are omitted for clarity). Selected interatomic distances (Å) and angles (deg): Pd−C1 1.994(4), Pd−P1 2.3072(12), Pd−P2 2.3020(12), Pd−O3 2.157(3), B1−O3 1.544(5), B1−O4 1.460(5), B1−O5 1.456(7), B1−O6 1.478(7); P1−Pd−P2 160.25(4), C1−Pd−O3 177.36(13), C1−Pd−P1 79.49(18), C1−Pd−P2 80.82(18), O3−B1−O4 102.4(3), O5−B1−O6 105.9(4), O3−Pd−P1 100.73(11), O3−Pd−P2 99.00(11).

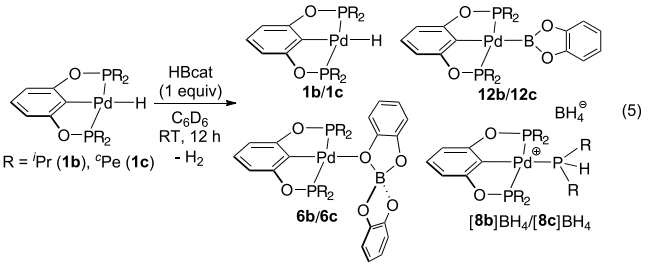

(5)

The cyclopentyl-substituted complex **1c** reacted with 1 equiv of HBcat in a similar fashion (eq 5); after 12 h, the products consisted of the unreacted hydride **1c** (15% of all pincer complexes), a boryl complex **12c** (40%), the bis(catecholato)-borate complex **6c** (23%), and the pincer degradation product [**8c**]BH$_4$ (22%). Pure **6c** was isolated, albeit in a low yield

https://doi.org/10.1021/acs.organomet.3c00126
Organometallics 2023, 42, 1525−1537

(32%), from a 2:1 reaction of HBcat with **1c** carried out in toluene (see Experimental Section for details). Further increasing the amount of HBcat (5−10 equiv with respect to **1c**) led to a higher conversion of **1c** to **12c** (>90%). Recrystallization of the crude products in diethyl ether produced a few single crystals of **12c**, which were studied crystallographically (Figure 6). The POCOP-pincer ligand

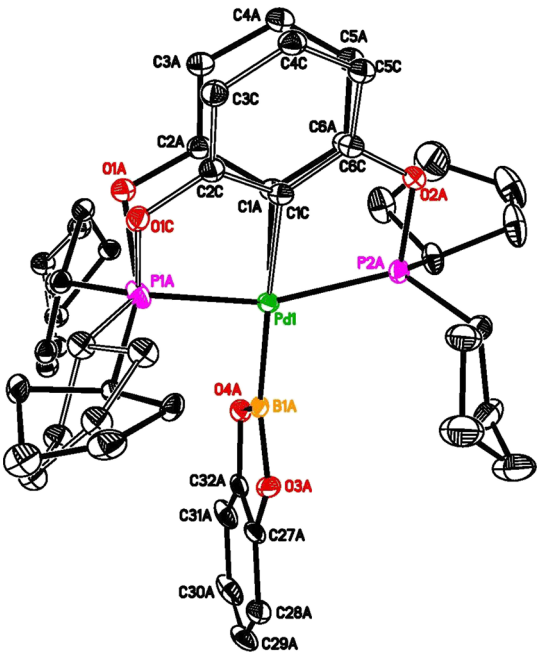

Figure 6. ORTEP of {2,6-(^{t}Pe$_2$PO)$_2$C$_6$H$_3$}PdBcat (**12c**), crystallized as two independent molecules with a disordered POCOP-pincer ligand. Molecule A is shown at 20% probability level (all hydrogen atoms are omitted for clarity). Selected interatomic distances (Å) and angles (deg): Pd1−C1A 2.04(3), Pd1−C1C 2.07(3), Pd1−P1A 2.2420(14), Pd1−P2A 2.2642(13), Pd1−B1A 2.068(5), B1A−O3A 1.430(7), B1A−O4A 1.412(7); P1A−Pd1−P2A 159.41(5), C1A−Pd1−B1A 175.2(6), C1C−Pd1−B1A 177.8(6), C1A−Pd1−P1A 79.7(8), C1C−Pd1−P1A 81.8(8), C1A−Pd1−P2A 79.9(8), C1C−Pd1−P2A 77.7(8), O3A−B1A−O4A 107.2(4), P1A−Pd1−B1A 99.31(15), P2A−Pd1−B1A 101.22(15).

shows substantial disorder for both independent molecules found in the crystal lattice (Figure S36). Nevertheless, the connectivity expected for **12c** was established. Isolating this boryl complex in a pure form proved to be difficult as it decomposed readily during work-up and purification. It should be noted that **12b**/**12c** was not detected from the reaction of **2b**/**2c** with HBcat (eq 3). Carbonyl insertion of HCO_2Bcat and HCHO into the hydride intermediate must be more competitive than the H_2 elimination reaction to produce **12b**/**12c**.

When studying palladium complexes bearing an amino-diphosphine-based pincer ligand, Ozerov and co-workers also observed H_2 elimination from the hydride species and HBcat to yield palladium boryl complexes (Scheme 4).[52] In that case, the reaction required heating overnight at 90 °C, likely due to the cationic nature of the hydride complexes. In contrast, the related neutral nickel hydride studied by the Mindiola group can undergo H_2 elimination with HBcat at room temperature.[51b] Our work here provides an opportunity to compare the reactivity of nickel and palladium hydrides strictly on the same pincer ligand platform. Unlike **1b** that reacts with HBcat

Scheme 4. Pincer-Stabilized Pd(II)/Ni(II) Boryl Complexes Formed via H_2 Elimination from the Hydride Derivatives and HBcat

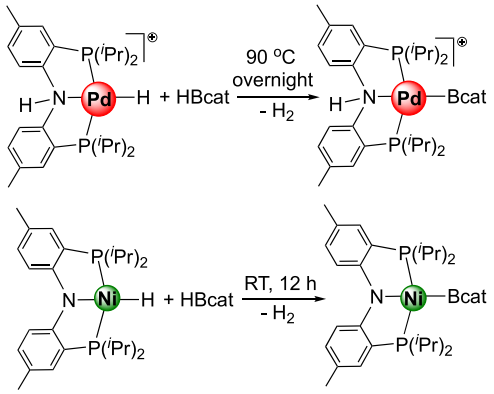

to generate multiple products including the palladium boryl complex **12b**, the nickel analog {2,6-(^{i}Pr$_2$PO)$_2$C$_6$H$_3$}NiH only forms a κ^2-H_2Bcat complex reversibly.[27d] In our previous studies of these two hydride complexes, we also showed distinctively different reaction patterns with phenylacetylene: **1b** favored H_2 elimination to yield an alkynyl species[36] whereas {2,6-(^{i}Pr$_2$PO)$_2$C$_6$H$_3$}NiH preferred insertion of the alkyne molecule into the Ni−H bond.[53] These results are consistent with the notion that the palladium center is more electron-rich, which increases the likelihood for the oxidative addition of H−Bcat or H−C≡CPh prior to H_2 elimination.

Implications in the Catalytic Reduction of CO_2. In a perfect scenario, the pincer-stabilized nickel or palladium hydride species is exclusively engaged in carbonyl insertion steps as outlined in Scheme 1, and the hydridic hydrogen in HBcat is fully utilized for CO_2 reduction. The formation of the bis(catecholato)borate complexes **6a−c** along with $B_2(cat)_3$ would lose some of the hydride to B_2H_6 which, during the catalytic process, can readily escape from the reaction mixture. The net boron redistribution reaction (3HBcat → $B_2(cat)_3$ + 1/2B_2H_6) could be catalyzed by the pincer complexes. This explains why the nickel catalysts **5a** and **5b** can achieve the maximum TON while other catalysts listed in Table 1 cannot. Among the catalytic systems examined here, these are the only two in which the corresponding bis(catecholato)borate complexes were not observed.

The formation of the secondary phosphine complexes such as [**8b**]BH_4 and [**8c**]BH_4 is expected to contribute to the demise of the catalysts. This type of degradation was particularly severe when **2b**, **2c**, and **5c** were employed as the catalysts. The P−O bonds in these complexes are more exposed and thus more susceptible to attack by HBcat.

The formation of the boryl complexes **12b** and **12c** plays a small, if any, role in the overall catalytic process, especially when there is a constant supply of CO_2. As implied by the stoichiometric studies (eq 3 vs eq 5), the hydride intermediates would choose carbonyl substrates over HBcat to react. However, the HBcat-first procedure might have converted some of the catalyst **2b**/**2c** to **12b**/**12c** before CO_2 was introduced. In the case of **2b**, the catalytic efficiency was unaffected by the addition order, suggesting that the formation of **12b** from **2b** and HBcat (in large excess) was comparatively slow. It is also possible that, under the catalytic conditions, the boryl complex may be converted back to the hydride complex

https://doi.org/10.1021/acs.organomet.3c00126
Organometallics 2023, 42, 1525−1537

via a palladium alkoxide intermediate generated from carbonyl insertion.[54]

For the nickel system, effects of phosphorus substituents on the catalytic reduction of CO_2 are significant (Table 1). The most efficient catalyst **5a** bears bulky *tert*-butyl groups on the phosphorus donors, which discourage the interaction of the nickel hydride with HBcat to form the catalytically dormant species, {2,6-(^{t}Bu$_2$PO)$_2$C$_6$H$_3$}Ni(κ^2-H$_2$Bcat). Reducing the steric congestion imposed by the pincer ligand can potentially increase the carbonyl insertion rates, as demonstrated by Hazari and co-workers in their kinetics study of CO_2 insertion into PCP-pincer-stabilized nickel hydrides.[55] However, CO_2 reduction to CH_3OBcat catalyzed by **5b** took a longer time to complete, presumably because the formation of a dihydridoborate complex is more favorable with the sterically less hindered hydride, {2,6-(^{i}Pr$_2$PO)$_2$C$_6$H$_3$}NiH.[27d] Catalyst **5c** has the same issue and at the same time suffers a rapid pincer degradation by HBcat, which explains why in this case the CO_2-first procedure gave a better result (entry 10 vs entry 9 in Table 1). Interestingly, these *P*-substituent effects are absent in the palladium system. With more electron-rich metal centers, the palladium hydride complexes have a lesser tendency to form adducts with HBcat to reduce the steady-state concentrations of the active species. The overall catalytic performance should be mainly determined by the carbonyl insertion steps. On steric grounds, we expect that **1b** and **1c** are more reactive palladium hydrides than **1a**. The higher reactivity toward CO_2, HCO_2Bcat, and HCHO is likely offset by a larger extent of catalyst decomposition as detailed earlier, leading to negligible differences observed for **2a**−**c** in catalyzing the reduction of CO_2 with HBcat.

CONCLUSIONS

Through this work, we have identified a number of traps that POCOP-type palladium pincer complexes can fall into during the catalytic reduction of CO_2 with HBcat. Compared to the nickel system, the palladium catalysts have more electron-rich metal centers, which disfavor the formation of κ^2-H$_2$Bcat complexes as the catalytically dormant species. However, the increased nucleophilicity for the palladium-bound X-type ligand creates a pathway for HBcat to be converted to $B_2(cat)_3$ and B_2H_6, resulting in a partial utilization of the borane for CO_2 reduction. Catalyst degradation initiated by P−O bond cleavage with HBcat is more severe in the palladium system when the phosphorus substituents are not sufficiently bulky. Another potential pitfall for the palladium catalysts is the formation of palladium boryl species via H_2 elimination from the palladium hydrides and HBcat, although such a transformation does not appear to be of major concern. Apart from P−O bond cleavage, which is unique to POCOP-pincer complexes, our findings here may be broadly implicated in other catalytic systems that employ HBcat, not just for the reduction of CO_2.

EXPERIMENTAL SECTION

General Methods. All organometallic compounds were prepared and handled under an argon atmosphere using standard glovebox and Schlenk techniques. Dry and oxygen-free solvents (toluene, pentane, diethyl ether, and tetrahydrofuran) were collected from an Innovative Technology solvent purification system and used throughout the experiments. Benzene and benzene-d_6 were dried over sodium-benzophenone and distilled under an argon atmosphere. HBcat was purified by vacuum distillation prior to use. ^{1}H, ^{13}C{^{1}H}, ^{31}P{^{1}H}, and ^{11}B{^{1}H} (or ^{11}B) NMR spectra were recorded on a Bruker AV400 or Bruker NEO400 NMR spectrometer. The chemical shift values for ^{1}H and ^{13}C{^{1}H} NMR spectra were referenced internally to the residual solvent resonances. ^{31}P{^{1}H} and ^{11}B{^{1}H} (or ^{11}B) NMR spectra were referenced externally to 85% H_3PO_4 (0 ppm) and $BF_3\cdot OEt_2$ (0 ppm), respectively. Infrared spectra were recorded on a Thermo Scientific Nicolet 6700 Fourier transform infrared (FT-IR) spectrometer equipped with smart orbit diamond attenuated total reflectance (ATR) accessory. {2,6-(R$_2$PO)$_2$C$_6$H$_3$}PdH (**1a**−**c**),[36] {2,6-(R$_2$PO)$_2$C$_6$H$_3$}PdCH$_3$ (**3a**−**c**),[36] {2,6-(R$_2$PO)$_2$C$_6$H$_3$}PdCl (**4b** and **4c**),[36] and {2,6-(R$_2$PO)$_2$C$_6$H$_3$}NiOCHO (**5a**−**c**)[27a,c] were prepared as described in the literature.

*Synthesis of {2,6-(^{t}Bu$_2$PO)$_2$C$_6$H$_3$}PdOCHO (**2a**).* Under an argon atmosphere, to a solution of **3a** (200 mg, 0.39 mmol) in 10 mL of toluene was added formic acid (95% purity, 18 μL, 0.45 mmol). The resulting mixture was stirred at room temperature for 15 min. The volatiles were removed under vacuum and the residue was washed with a small amount of cold pentane. The desired product was isolated as a white solid (128 mg, 60% yield) after being exposed to vacuum conditions for a short period of time. Extensive drying under vacuum (>1 h) should be avoided as the formate complex will undergo decarboxylation. If needed, this compound can be further purified via recrystallization in toluene at −30 °C. ^{1}H NMR (400 MHz, C$_6$D$_6$): δ 8.93 (t, $^4J_{H-P}$ = 1.6 Hz, PdOC*H*O, 1H), 6.88−6.82 (m, Ar*H*, 1H), 6.63 (d, $^3J_{H-H}$ = 8.0 Hz, Ar*H*, 2H), 1.38−1.29 (m, C*H*$_3$, 36H). ^{1}H NMR (400 MHz, CDCl$_3$): δ 8.45 (t, $^4J_{H-P}$ = 1.4 Hz, PdOC*H*O, 1H), 6.94 (t, $^3J_{H-H}$ = 8.0 Hz, Ar*H*, 1H), 6.51 (d, $^3J_{H-H}$ = 8.0 Hz, Ar*H*, 2H), 1.39 (vt, J_{H-P} = 15.2 Hz, C*H*$_3$, 36H). ^{13}C{^{1}H} NMR (101 MHz, CDCl$_3$): δ 167.7 (s, PdOCHO), 167.4 (vt, J_{C-P} = 12.5 Hz, ArC$_{ortho}$), 127.8 (s, ArC$_{para}$), 125.9 (t,$^2J_{C-P}$ = 3.3 Hz, ArC$_{ipso}$), 105.9 (vt, J_{C-P} = 13.8 Hz, ArC$_{meta}$), 39.4 (vt, J_{C-P} = 14.6 Hz, *C*(CH$_3$)$_3$), 27.5 (vt, J_{C-P} = 8.3 Hz, CH$_3$). ^{31}P{^{1}H} NMR (162 MHz, C$_6$D$_6$): δ 192.0 (s). ^{31}P{^{1}H} NMR (162 MHz, CDCl$_3$): δ 191.5 (s). Selected ATR-IR data (solid, cm^{-1}): 2962, 2900, 2868, 2771, 1624, 1579, 1565, 1472, 1442, 1369, 1310, 1247, 1224, 1182. Anal. Calcd for C$_{23}$H$_{40}$O$_4$P$_2$Pd: C, 50.32; H, 7.34. Found: C, 50.04; H, 7.26.

*Synthesis of {2,6-(^{i}Pr$_2$PO)$_2$C$_6$H$_3$}PdOCHO (**2b**).* Under an argon atmosphere, to a solution of **3b** (200 mg, 0.43 mmol) in 10 mL of toluene was added formic acid (95% purity, 20 μL, 0.50 mmol). The resulting mixture was stirred at room temperature for 15 min. The volatiles were removed under vacuum and the residue was extracted with pentane (60 mL). Evaporation of the pentane solution afforded the product as a faint yellow solid (97 mg, 46% yield). Extensive drying under vacuum (>1 h) should be avoided as the formate complex will undergo decarboxylation. If needed, this compound can be further purified via recrystallization from a saturated pentane solution kept at −30 °C. ^{1}H NMR (400 MHz, C$_6$D$_6$): δ 8.76 (s, PdOC*H*O, 1H), 6.87 (t, $^3J_{H-H}$ = 8.0 Hz, Ar*H*, 1H), 6.66 (d, $^3J_{H-H}$ = 8.0 Hz, Ar*H*, 2H), 2.47−2.26 (m, C*H*(CH$_3$)$_2$, 4H), 1.41−1.20 (m, C*H*$_3$, 12H), 1.20−1.03 (m, C*H*$_3$, 12H). ^{13}C{^{1}H} NMR (101 MHz, C$_6$D$_6$): δ 167.3 (vt, J_{C-P} = 13.1 Hz, ArC$_{ortho}$), 166.3 (s, PdOCHO), 128.6 (s, ArC$_{para}$), 126.9 (t,$^2J_{C-P}$ = 4.0 Hz, ArC$_{ipso}$), 106.2 (vt, J_{C-P} = 14.1 Hz, ArC$_{meta}$), 29.8 (vt, J_{C-P} = 24.2 Hz, CH(CH$_3$)$_2$), 18.0 (vt, J_{C-P} = 8.3 Hz, CH$_3$), 16.9 (s, CH$_3$). ^{31}P{^{1}H} NMR (162 MHz, C$_6$D$_6$): δ 187.3 (s). Selected ATR-IR data (solid, cm^{-1}): 2958, 1594, 1566, 1440, 1424, 1292, 1236, 1218. Anal. Calcd for C$_{19}$H$_{32}$O$_4$P$_2$Pd: C, 46.31; H, 6.54. Found: C, 46.33; H, 6.48.

*Synthesis of {2,6-(^{c}Pe$_2$PO)$_2$C$_6$H$_3$}PdOCHO (**2c**).* This compound was prepared in 49% yield by a procedure similar to that used for **2b**. ^{1}H NMR (400 MHz, C$_6$D$_6$): δ 8.77 (s, PdOC*H*O, 1H), 6.88 (t, $^3J_{H-H}$ = 8.0 Hz, Ar*H*, 1H), 6.70 (d, $^3J_{H-H}$ = 8.0 Hz, Ar*H*, 2H), 2.73−2.54 (m, PC*H*, 4H), 2.14−1.85 (m, C*H*$_2$, 12H), 1.81−1.53 (m, C*H*$_2$, 12H), 1.48−1.27 (m, C*H*$_2$, 8H). ^{13}C{^{1}H} NMR (101 MHz, C$_6$D$_6$): δ 167.2 (vt, J_{C-P} = 13.2 Hz, ArC$_{ortho}$), 166.2 (s, PdOCHO), 128.6 (s, ArC$_{para}$), 126.8 (t,$^2J_{C-P}$ = 3.8 Hz, ArC$_{ipso}$), 106.2 (vt, J_{C-P} = 13.2 Hz, ArC$_{meta}$), 40.6 (vt, J_{C-P} = 26.5 Hz, PCH), 28.7 (vt, J_{C-P} = 9.0 Hz, CH$_2$), 28.3 (s, CH$_2$), 26.8 (vt, J_{C-P} = 7.0 Hz, CH$_2$), 26.5 (vt, J_{C-P} = 9.0 Hz, CH$_2$). ^{31}P{^{1}H} NMR (162 MHz, C$_6$D$_6$): δ 176.7 (s). Selected ATR-IR data (solid, cm^{-1}): 2954, 2864, 1599, 1580, 1567, 1440,

https://doi.org/10.1021/acs.organomet.3c00126
Organometallics 2023, 42, 1525−1537

1425, 1298, 1425, 1298, 1234, 1218. Anal. Calcd for $C_{27}H_{40}O_4P_2Pd$: C, 54.32; H, 6.75. Found: C, 54.33; H, 6.64.

Catalytic Reduction of CO_2 with HBcat. *HBcat-First Method.* Under an argon atmosphere, a flame-dried Schlenk flask was charged with a palladium or nickel catalyst (25 μmol), hexamethyldisilane (10.4 μL, 50 μmol), and 2.0 mL of C_6D_6. To this solution, HBcat (272 μL, 2.5 mmol) was added. CO_2 was then introduced to the reaction mixture via the freeze-pump-thaw method. The reaction was stirred at room temperature under 1 atm of CO_2. After an appropriate time, an aliquot of the mixture was withdrawn for NMR analysis.

CO_2-First Method. Under an argon atmosphere, a flame-dried Schlenk flask was charged with a palladium or nickel catalyst (25 μmol), hexamethyldisilane (10.4 μL, 50 μmol), and 2.0 mL of C_6D_6. The argon inside the flask was replaced with CO_2 using the freeze-pump-thaw method. HBcat (272 μL, 2.5 mmol) was then added to the reaction mixture. The reaction was stirred at room temperature under 1 atm of CO_2. After an appropriate time, an aliquot of the mixture was withdrawn for NMR analysis.

Stoichiometric Reduction of Palladium Formate Complexes with HBcat. Under an argon atmosphere, a palladium formate complex (25 μmol), hexamethyldisilane (1.7 μL, 8.0 μmol), and 0.5 mL of C_6D_6 were mixed in a J. Young NMR tube. To the resulting solution, HBcat (8.2 μL, 75 μmol) was added and the progress of the reaction was monitored by NMR spectroscopy.

*Synthesis of {2,6-(^{t}Bu$_2$PO)$_2$C$_6$H$_3$}PdB(cat)$_2$ (**6a**).* Under an argon atmosphere, to a solution of **1a** (200 mg, 0.40 mmol) in 10 mL of toluene was slowly added HBcat (3.23 mL, 30 mmol). The mixture was first stirred at room temperature for 30 min and then concentrated under vacuum. The resulting white solid was washed with 30 mL of pentane followed by extraction with 20 mL of diethyl ether. Evaporation of the solvent from the etherate solution gave a white solid, which was kept under dynamic vacuum for at least 24 h. The solid was then dissolved in 3 mL of toluene and layered with 6 mL of diethyl ether at which point gas evolution was noted. After being left to stand for 1 h, the solution was pumped to dryness. The desired product was further enriched by recrystallization in benzene at room temperature and isolated as a white solid (60 mg, <20% yield). Despite repeated trials, the isolated solid always contained some $B_2(cat)_3$. ^{1}H NMR (400 MHz, C_6D_6): δ 7.12−7.01 (m, Ar*H*, 4H), 6.86−6.79 (m, Ar*H*, 4H), 6.78−6.72 (m, Ar*H*, 1H), 6.44 (d, $^3J_{H-H}$ = 8.0 Hz, Ar*H*, 2H), 1.15 (vt, J_{H-P} = 15.6 Hz, C*H*$_3$, 36H). ^{13}C{^{1}H} NMR (101 MHz, C_6D_6): δ 167.3 (vt, J_{C-P} = 10.1 Hz, ArC$_{ortho}$), 151.7 (s, ArC$_{cat}$), 129.5 (s, ArC$_{para}$), 120.6 (s, ArC$_{ipso}$), 119.4 (s, ArC$_{cat}$), 111.0 (s, ArC$_{cat}$), 106.6 (vt, J_{C-P} = 13.1 Hz, ArC$_{meta}$), 39.8 (vt, J_{C-P} = 14.1 Hz, C(CH$_3$)$_3$), 27.3 (vt, J_{C-P} = 7.0 Hz, CH$_3$). ^{31}P{^{1}H} NMR (162 MHz, C_6D_6): δ 192.2 (s). ^{11}B{^{1}H} NMR (128 MHz, C_6D_6): δ 14.5 (s). Anal. Calcd for $C_{34}H_{47}BO_6P_2Pd$: C, 55.87; H, 6.48. Found: C, 57.74; H, 6.63. Although these results are outside the range viewed as establishing analytical purity, they are provided to illustrate the best values obtained to date.

*Synthesis of {2,6-(^{i}Pr$_2$PO)$_2$C$_6$H$_3$}PdB(cat)$_2$ (**6b**).* Under an argon atmosphere, to a solution of **1b** (100 mg, 0.22 mmol) in 10 mL of toluene was added HBcat (27 μL, 0.25 mmol). The mixture was stirred at room temperature for 12 h after which it was placed under vacuum conditions for a prolonged period of time (12 h) to remove all volatiles. The residue was washed with 10 mL of pentane and then treated with 1 mL of benzene. The resulting mixture was filtered through a Pasteur pipette filled with Celite, and the filtrate was kept at room temperature. After 24 h, the product precipitated out of the solution as colorless crystals (25 mg, 17% yield). ^{1}H NMR (400 MHz, C_6D_6): δ 7.05−6.96 (m, Ar*H*, 4H), 6.84−6.78 (m, Ar*H*, 4H), 6.75 (t, $^3J_{H-H}$ = 8.0 Hz, Ar*H*, 1H), 6.49 (d, $^3J_{H-H}$ = 8.0 Hz, Ar*H*, 2H), 2.20−2.09 (m, C*H*(CH$_3$)$_2$, 4H), 1.08−0.98 (m, C*H*$_3$, 12H), 0.98−0.87 (m, C*H*$_3$, 12H). ^{13}C{^{1}H} NMR (101 MHz, C_6D_6): δ 167.2 (vt, J_{C-P} = 10.3 Hz, ArC$_{ortho}$), 151.7 (s, ArC$_{cat}$), 129.7 (s, ArC$_{para}$), 122.2 (s, ArC$_{ipso}$), 119.5 (s, ArC$_{cat}$), 110.1 (s, ArC$_{cat}$), 106.9 (vt, J_{C-P} = 13.8 Hz, ArC$_{meta}$), 28.9 (vt, J_{C-P} = 22.9 Hz, CH(CH$_3$)$_2$), 16.4 (vt, J_{C-P} = 7.7 Hz, CH$_3$), 16.0 (s, CH$_3$). ^{31}P{^{1}H} NMR (162 MHz, C_6D_6): δ 186.8 (s). ^{11}B{^{1}H} NMR (128 MHz, C_6D_6): δ 14.4 (s). Anal. Calcd for $C_{30}H_{39}BO_6P_2Pd$: C, 53.40; H, 5.83. Found: C, 53.13; H, 5.97.

*Synthesis of {2,6-(^{c}Pe$_2$PO)$_2$C$_6$H$_3$}PdB(cat)$_2$ (**6c**).* Under an argon atmosphere, to a solution of **1c** (200 mg, 0.36 mmol) in 10 mL of toluene was added HBcat (78 μL, 0.72 mmol). The mixture was stirred at room temperature for 12 h after which it was placed under vacuum conditions for a prolonged period of time (12 h) to remove all volatiles. The residue was extracted with 40 mL of diethyl ether. The resulting etherate solution was pumped to dryness and then left under vacuum for 12 h. Treatment of the obtained solid with 1 mL of benzene followed by filtration through a Pasteur pipette filled with Celite gave a clear solution. After being left to stand for 24 h, the solution yielded some colorless crystals of the desired product (89 mg, 32% yield). ^{1}H NMR (400 MHz, C_6D_6): δ 7.02−6.90 (m, Ar*H*, 4H), 6.80 (t, $^3J_{H-H}$ = 8.0 Hz, Ar*H*, 1H), 6.76−6.67 (m, Ar*H*, 4H), 6.54 (d, $^3J_{H-H}$ = 8.0 Hz, Ar*H*, 2H), 2.47−2.23 (m, PC*H*, 4H), 1.99−1.75 (m, C*H*$_2$, 4H), 1.75−1.43 (m, C*H*$_2$, 16H), 1.41−1.21 (m, C*H*$_2$, 12H). ^{13}C{^{1}H} NMR (101 MHz, C_6D_6): δ 166.9 (vt, J_{C-P} = 12.1 Hz, ArC$_{ortho}$), 151.3 (s, ArC$_{cat}$), 129.8 (s, ArC$_{para}$), 122.2 (t, J_{C-P} = 6.5 Hz, ArC$_{ipso}$), 119.6 (s, ArC$_{cat}$), 110.1 (s, ArC$_{cat}$), 106.9 (vt, J_{C-P} = 13.9 Hz, ArC$_{meta}$), 40.5 (vt, J_{C-P} = 25.7 Hz, PCH), 28.5 (s, CH$_2$), 27.7 (vt, J_{C-P} = 8.1 Hz, CH$_2$), 26.6 (vt, J_{C-P} = 9.2 Hz, CH$_2$), 26.0 (vt, J_{C-P} = 11.0 Hz, CH$_2$). ^{31}P{^{1}H} NMR (162 MHz, C_6D_6): δ 179.4 (s). ^{11}B{^{1}H} NMR (128 MHz, C_6D_6): δ 14.5 (s). Anal. Calcd for $C_{38}H_{47}BO_6P_2Pd$: C, 58.59; H, 6.08. Found: C, 58.93; H, 6.44.

*Synthesis of [{2,6-(^{i}Pr$_2$PO)$_2$C$_6$H$_3$}Pd(HP^{i}Pr$_2$)]OTf ([**8b**]OTf).* Under an argon atmosphere, to a solution of **4b** (48 mg, 0.10 mmol) in 2 mL of tetrahydrofuran was added silver triflate (31 mg, 0.12 mmol). The reaction mixture was kept in the dark and stirred for 2 h before being filtered through a short pad of Celite. To the filtrate, a 10 wt % solution of HP^{i}Pr$_2$ in hexane (119 mg, 0.10 mmol) was added and the resulting mixture was stirred for 10 min. Removal of the volatiles under reduced pressure afforded an off-white residue, which was washed with 5 mL of pentane and then dried under vacuum. The desired product was isolated as a white powder (50 mg, 70% yield). ^{1}H NMR (400 MHz, C_6D_6): δ 6.89 (t, $^3J_{H-H}$ = 8.0 Hz, Ar*H*, 1H), 6.64 (d, $^3J_{H-H}$ = 8.0 Hz, Ar*H*, 2H), 4.99 (dm, $^1J_{H-P}$ = 340.0 Hz, P*H*, 1H), 2.68−2.52 (m, PC*H*, 4H), 2.51−2.35 (m, PC*H*, 2H), 1.55−1.42 (m, C*H*$_3$, 6H), 1.33−1.20 (m, C*H*$_3$, 6H), 1.20−1.06 (m, C*H*$_3$, 24H). ^{13}C{^{1}H} NMR (101 MHz, C_6D_6): δ 166.0 (vt, J_{C-P} = 9.6 Hz, ArC$_{ortho}$), 137.6 (d, $^2J_{C-P}$ = 81.4 Hz, ArC$_{ipso}$), 131.2 (s, ArC$_{para}$), 122.6 (q, $^1J_{C-F}$ = 323.8 Hz, CF$_3$), 106.2 (vt, J_{C-P} = 14.2 Hz, ArC$_{meta}$), 30.5 (vt, J_{C-P} = 25.6 Hz, PCH), 24.3 (d, $^1J_{C-P}$ = 23.9 Hz, PCH), 22.3 (d, $^2J_{C-P}$ = 3.9 Hz, CH$_3$), 21.9 (d, $^2J_{C-P}$ = 5.1 Hz, CH$_3$), 18.0 (s, CH$_3$), 16.8 (s, CH$_3$). ^{31}P{^{1}H} NMR (162 MHz, C_6D_6): δ 197.8 (d, $^2J_{P-P}$ = 32.4 Hz, OP^{i}Pr$_2$, 2P), 1.1 (t, $^2J_{P-P}$ = 32.4 Hz, HP^{i}Pr$_2$, 1P). Anal. Calcd for $C_{25}H_{46}O_5F_3P_3SPd$: C, 41.99; H, 6.48. Found: C, 42.26; H, 6.39.

*Synthesis of [{2,6-(^{c}Pe$_2$PO)$_2$C$_6$H$_3$}Pd(HP^{c}Pe$_2$)]OTf ([**8c**]OTf).* This compound was prepared in 49% yield by a procedure similar to that used for [**8b**]OTf. ^{1}H NMR (400 MHz, C_6D_6): δ 6.90 (t, $^3J_{H-H}$ = 8.0 Hz, Ar*H*, 1H), 6.70 (dd, $^3J_{H-H}$ = 8.0 Hz, $^5J_{H-P}$ = 2.0 Hz, Ar*H*, 2H), 5.11 (dm, $^1J_{H-P}$ = 342.8 Hz, P*H*, 1H), 3.12−2.85 (m, PC*H*, 4H), 2.82−2.64 (m, PC*H*, 2H), 2.63−2.45 (m, C*H*$_2$, 2H), 2.28−1.39 (m, C*H*$_2$, 46H). ^{13}C{^{1}H} NMR (101 MHz, C_6D_6): δ 166.3 (vt, J_{C-P} = 9.2 Hz, ArC$_{ortho}$), 137.8 (d, $^2J_{C-P}$ = 80.8 Hz, ArC$_{ipso}$), 130.8 (s, ArC$_{para}$), 122.5 (q, $^1J_{C-F}$ = 324.0 Hz, CF$_3$), 106.2 (vt, J_{C-P} = 13.2 Hz, ArC$_{meta}$), 41.5 (vt, J_{C-P} = 27.8 Hz, PCH), 34.8 (d, $^1J_{C-P}$ = 26.3 Hz, PCH), 34.5 (d, J_{C-P} = 5.2 Hz, CH$_2$), 33.3 (d, J_{C-P} = 6.2 Hz, CH$_2$), 30.4 (s, CH$_2$), 28.4 (s, CH$_2$), 26.9 (br, CH$_2$), 26.6 (d, J_{C-P} = 7.8 Hz, CH$_2$), 26.2 (vt, J_{C-P} = 10.1 Hz, CH$_2$), 25.9 (d, J_{C-P} = 11.3 Hz, CH$_2$). ^{31}P{^{1}H} NMR (162 MHz, C_6D_6): δ 186.2 (d, $^2J_{P-P}$ = 30.2 Hz, OP^{c}Pe$_2$, 2P), −4.7 (t, $^2J_{P-P}$ = 30.2 Hz, HP^{c}Pe$_2$, 1P). Anal. Calcd for $C_{37}H_{58}O_5F_3P_3SPd$: C, 51.01; H, 6.71. Found: C, 51.29; H, 6.85.

NMR Data of 12c (Generated in Situ). The NMR sample was prepared by mixing **1c** with ∼10 equiv of HBcat in C_6D_6 for 12 h (at RT). ^{1}H NMR (400 MHz, C_6D_6): δ 7.30−7.25 (m, Ar*H*, 4H), 7.07 (t, $^3J_{H-H}$ = 8.0 Hz, Ar*H*, 1H), 7.01−6.95 (m, Ar*H* of HBcat), 6.87−6.83 (m, Ar*H*, 4H), 6.78−6.71 (m, Ar*H* of HBcat), 4.56 (q, $^1J_{H-B}$ = 188 Hz, *H*Bcat), 4.47 (s, H$_2$), 2.39−2.24 (m, PC*H*, 4H), 2.00−1.22 (m, C*H*$_2$); one of the aromatic resonances for **12c** was obscured by HBcat resonances. ^{13}C{^{1}H} NMR (101 MHz, C_6D_6): δ 165.4 (vt, J_{C-P} = 13.6 Hz, ArC$_{ortho}$), 150.4 (s, ArC$_{cat}$), 147.9 (s, Ar*C* of HBcat),

https://doi.org/10.1021/acs.organomet.3c00126
Organometallics 2023, 42, 1525−1537

129.4 (s, ArC_{para}), 123.2 (s, ArC of HBcat), 122.8 (s, ArC_{ipso}), 121.5 (s, ArC_{cat}), 112.9 (s, ArC of HBcat), 111.5 (s, ArC_{cat}), 105.3 (vt, J_{C-P} = 13.8 Hz, ArC_{meta}), 40.6 (vt, J_{C-P} = 29.2 Hz, PCH), 29.1 (s, CH_2), 28.8 (vt, J_{C-P} = 9.8 Hz, CH_2), 26.8 (vt, J_{C-P} = 7.0 Hz, CH_2), 26.7 (vt, J_{C-P} = 8.7 Hz, CH_2). $^{31}P\{^1H\}$ NMR (162 MHz, C_6D_6): δ 191.8 (s). $^{11}B\{^1H\}$ NMR (128 MHz, C_6D_6): δ 50.8 (br, **12c**), 28.8 (s, HBcat), 22.5 (br, $B_2(cat)_3$).

X-ray Structure Determinations. To obtain X-ray quality crystals, saturated solutions of **2a** (in toluene), **2b** (in pentane), and [**8b**]OTf (in toluene) were kept at −30 °C. Single crystals of **6a** and **6b** were obtained when the NMR samples (in C_6D_6) were left at room temperature overnight. Single crystals of **12c** were obtained from slow evaporation of a diethyl ether solution, which was prepared by extracting the crude product from the reaction of **1c** with 10 equiv of HBcat. Crystal data collection and refinement parameters are provided in the Supporting Information. The intensity data were collected at 150 K on a Bruker SMART6000 CCD diffractometer using graphite-monochromated Cu Kα radiation, λ = 1.54178 Å. The data frames were processed using the program SAINT. The data were corrected for decay, Lorentz, and polarization effects as well as absorption and beam corrections based on the multiscan technique. The structures were solved by a combination of direct or Patterson methods in SHELXTL and the difference Fourier technique and refined by full-matrix least-squares procedures. Non-hydrogen atoms were refined with anisotropic displacement parameters. The H-atoms were calculated and treated with a riding model. The H-atom isotropic displacement parameters were defined as $a \times U_{eq}$ (a = 1.5 for methyl and 1.2 for all others) of the adjacent atom. Substantial disorder in the POCOP-pincer ligand for both independent molecules of **12c** was refined with a multicomponent model which required distance and anisotropic displacement parameter restraints. **6a** co-crystallizes with a C_6D_6 molecule in the lattice. The C_6D_6 molecule shows some disorder; however, no multicomponent disorder model was applied. For the remaining structures, no solvent of crystallization is present in the lattice.

■ ASSOCIATED CONTENT

Supporting Information

The Supporting Information is available free of charge at https://pubs.acs.org/doi/10.1021/acs.organomet.3c00126.

NMR and IR spectra of the palladium complexes and more detailed X-ray crystallographic information (PDF)

Accession Codes

CCDC 2246391−2246396 contain the supplementary crystallographic data for this paper. These data can be obtained free of charge via www.ccdc.cam.ac.uk/data_request/cif, or by emailing data_request@ccdc.cam.ac.uk, or by contacting The Cambridge Crystallographic Data Centre, 12 Union Road, Cambridge CB2 1EZ, UK; fax: +44 1223 336033.

■ AUTHOR INFORMATION

Corresponding Authors

Anubendu Adhikary − *School of Advanced Sciences, VIT-AP University, Amaravati, Andhra Pradesh 522237, India*; Email: anubendu.a@vitap.ac.in

Hairong Guan − *Department of Chemistry, University of Cincinnati, Cincinnati, Ohio 45221-0172, United States*; orcid.org/0000-0002-4858-3159; Email: hairong.guan@uc.edu

Authors

Sayantani Saha − *Department of Chemistry, University of Cincinnati, Cincinnati, Ohio 45221-0172, United States*

N. Sai Kumar − *School of Advanced Sciences, VIT-AP University, Amaravati, Andhra Pradesh 522237, India*

Allen G. Oliver − *Department of Chemistry & Biochemistry, University of Notre Dame, Notre Dame, Indiana 46556, United States*; orcid.org/0000-0002-0511-1127

Jeanette A. Krause − *Department of Chemistry, University of Cincinnati, Cincinnati, Ohio 45221-0172, United States*

Complete contact information is available at: https://pubs.acs.org/10.1021/acs.organomet.3c00126

Notes

The authors declare no competing financial interest.

■ ACKNOWLEDGMENTS

We thank the NSF Chemical Catalysis Program for supporting this research project (CHE-0952083 and CHE-2102192) and the NSF MRI Program for supporting the instrumentation used in this study, which includes a Bruker SMART6000 CCD diffractometer (CHE-0215950) and a Bruker NEO400 MHz NMR spectrometer (CHE-1726092).

■ REFERENCES

(1) (a) Arakawa, H.; Aresta, M.; Armor, J. N.; Barteau, M. A.; Beckman, E. J.; Bell, A. T.; Bercaw, J. E.; Creutz, C.; Dinjus, E.; Dixon, D. A.; Domen, K.; DuBois, D. L.; Eckert, J.; Fujita, E.; Gibson, D. H.; Goddard, W. A.; Goodman, D. W.; Keller, J.; Kubas, G. J.; Kung, H. H.; Lyons, J. E.; Manzer, L. E.; Marks, T. J.; Morokuma, K.; Nicholas, K. M.; Periana, R.; Que, L.; Rostrup-Nielson, J.; Sachtler, W. M. H.; Schmidt, L. D.; Sen, A.; Somorjai, G. A.; Stair, P. C.; Stults, B. R.; Tumas, W. Catalysis Research of Relevance to Carbon Management: Progress, Challenges, and Opportunities. *Chem. Rev.* **2001**, *101*, 953−996. (b) Peter, S. C. Reduction of CO_2 to Chemicals and Fuels: A Solution to Global Warming and Energy Crisis. *ACS Energy Lett.* **2018**, *3*, 1557−1561. (c) Cheon, J.; Yang, J. Y.; Koper, M.; Ishitani, O. From Pollutant to Chemical Feedstock: Valorizing Carbon Dioxide through Photo- and Electrochemical Processes. *Acc. Chem. Res.* **2022**, *55*, 931−932.

(2) Homogeneous catalysts: (a) Wang, W.-H.; Himeda, Y.; Muckerman, J. T.; Manbeck, G. F.; Fujita, E. CO_2 Hydrogenation to Formate and Methanol as an Alternative to Photo- and Electrochemical CO_2 Reduction. *Chem. Rev.* **2015**, *115*, 12936−12973. (b) Bernskoetter, W. H.; Hazari, N. Reversible Hydrogenation of Carbon Dioxide to Formic Acid and Methanol: Lewis Acid Enhancement of Base Metal Catalysts. *Acc. Chem. Res.* **2017**, *50*, 1049−1058. (c) Grice, K. A. Carbon Dioxide Reduction with Homogeneous Early Transition Metal Complexes: Opportunities and Challenges for Developing CO_2 Catalysis. *Coord. Chem. Rev.* **2017**, *336*, 78−95.

(3) Heterogeneous catalysts: (a) Porosoff, M. D.; Yan, B.; Chen, J. G. Catalytic Reduction of CO_2 by H_2 for Synthesis of CO, Methanol and Hydrocarbons: Challenges and Opportunities. *Energy Environ. Sci.* **2016**, *9*, 62−73. (b) Ye, R.-P.; Ding, J.; Gong, W.; Aygyle, M. D.; Zhong, Q.; Wang, Y.; Russell, C. K.; Xu, Z.; Russell, A. G.; Li, Q.; Fan, M.; Yao, Y.-G. CO_2 Hydrogenation to High-Value Products via Heterogeneous Catalysis. *Nat. Commun.* **2019**, *10*, 5698. (c) Modak, A.; Bhanja, P.; Dutta, S.; Chowdhury, B.; Bhaumik, A. Catalytic Reduction of CO_2 into Fuels and Fine Chemicals. *Green Chem.* **2020**, *22*, 4002−4033. (d) Jiang, X.; Nie, X.; Guo, X.; Song, C.; Chen, J. G. Recent Advances in Carbon Dioxide Hydrogenation to Methanol via Heterogeneous Catalysis. *Chem. Rev.* **2020**, *120*, 7984−8034.

(4) (a) Takeda, H.; Cometto, C.; Ishitani, O.; Robert, M. Electrons, Photons, Protons and Earth-Abundant Metal Complexes for Molecular Catalysis of CO_2 Reduction. *ACS Catal.* **2017**, *7*, 70−88. (b) Wu, J.; Huang, Y.; Ye, W.; Li, Y. CO_2 Reduction: From the Electrochemical to Photochemical Approach. *Adv. Sci.* **2017**, *4*, No. 1700194. (c) Grills, D. C.; Ertem, M. Z.; McKinnon, M.; Ngo, K. T.; Rochford, J. Mechanistic Aspects of CO_2 Reduction Catalysis with Manganese-Based Molecular Catalysts. *Coord. Chem. Rev.* **2018**, *374*,

173−217. (d) Cauwenbergh, R.; Das, S. Photochemical Reduction of Carbon Dioxide to Formic Acid. *Green Chem.* **2021**, *23*, 2553−2574.
(5) (a) Benson, E. E.; Kubiak, C. P.; Sathrum, A. J.; Smieja, J. M. Electrocatalytic and Homogeneous Approaches to Conversion of CO_2 to Liquid Fuels. *Chem. Soc. Rev.* **2009**, *38*, 89−99. (b) Costentin, C.; Robert, M.; Savéant, J.-M. Catalysis of the Electrochemical Reduction of Carbon Dioxide. *Chem. Soc. Rev.* **2013**, *42*, 2423−2436. (c) Qiao, J.; Liu, Y.; Hong, F.; Zhang, J. A Review of Catalysts for the Electroreduction of Carbon Dioxide to Produce Low-Carbon Fuels. *Chem. Soc. Rev.* **2014**, *43*, 631−675. (d) Loewen, N. D.; Neelakantan, T. V.; Berben, L. A. Renewable Formate from C−H Bond Formation with CO_2: Using Iron Carbonyl Clusters as Electrocatalysts. *Acc. Chem. Res.* **2017**, *50*, 2362−2370. (e) Elgrishi, N.; Chambers, M. B.; Wang, X.; Fontecave, M. Molecular Polypyridine-Based Metal Complexes as Catalysts for the Reduction of CO_2. *Chem. Soc. Rev.* **2017**, *46*, 761−796. (f) Francke, R.; Schille, B.; Roemelt, M. Homogeneously Catalyzed Electroreduction of Carbon Dioxide − Methods, Mechanisms, and Catalysts. *Chem. Rev.* **2018**, *118*, 4631−4701. (g) Resasco, J.; Bell, A. T. Electrocatalytic CO_2 Reduction to Fuels: Progress and Opportunities. *Trends Chem.* **2020**, *2*, 825−836. (h) Zhang, X.; Guo, S.-X.; Gandionco, K. A.; Bond, A. M.; Zhang, J. Electrocatalytic Carbon Dioxide Reduction: from Fundamental Principles to Catalyst Design. *Mater. Today Adv.* **2020**, *7*, No. 100074. (i) Bonetto, R.; Crisanti, F.; Sartorel, A. Carbon Dioxide Reduction Mediated by Iron Catalysts: Mechanism and Intermediates That Guide Selectivity. *ACS Omega* **2020**, *5*, 21309−21319.
(6) (a) Bontemps, S.; Vendier, L.; Sabo-Etienne, S. Ruthenium-Catalyzed Reduction of Carbon Dioxide to Formaldehyde. *J. Am. Chem. Soc.* **2014**, *136*, 4419−4425. (b) Jin, G.; Werncke, C. G.; Escudié, Y.; Sabo-Etienne, S.; Bontemps, S. Iron-Catalyzed Reduction of CO_2 into Methylene: Formation of C−N, C−O, and C−C Bonds. *J. Am. Chem. Soc.* **2015**, *137*, 9563−9566. (c) Murphy, L. J.; Hollenhorst, H.; McDonald, R.; Ferguson, M.; Lumsden, M. D.; Turculet, L. Selective Ni-Catalyzed Hydroboration of CO_2 to the Formaldehyde Level Enabled by New PSiP Ligation. *Organometallics* **2017**, *36*, 3709−3720.
(7) Stoichiometric reduction of CO_2 with $NaBH_4$: (a) Fujiwara, K.; Yasuda, S.; Mizuta, T. Reduction of CO_2 to Trimethoxyboroxine with BH_3 in THF. *Organometallics* **2014**, *33*, 6692−6695. (b) Knopf, I.; Cummins, C. C. Revisiting CO_2 Reduction with $NaBH_4$ under Aprotic Conditions: Synthesis and Characterization of Sodium Triformatoborohydride. *Organometallics* **2015**, *34*, 1601−1603.
(8) Stoichiometric reduction of CO_2 with other borohydrides: (a) Ashley, A. E.; Thompson, A. L.; O'Hare, D. Non-Metal-Mediated Homogeneous Hydrogenation of CO_2 to CH_3OH. *Angew. Chem., Int. Ed.* **2009**, *48*, 9839−9843. (b) Berkefeld, A.; Piers, W. E.; Parvez, M. Tandem Frustrated Lewis Pair/Tris(pentafluorophenyl)borane-Catalyzed Deoxygenative Hydrosilylation of Carbon Dioxide. *J. Am. Chem. Soc.* **2010**, *132*, 10660−10661. (c) Anker, M. D.; Arrowsmith, M.; Bellham, P.; Hill, M. S.; Kociok-Köhn, G.; Liptrot, D. J.; Mahon, M. F.; Weetman, C. Selective Reduction of CO_2 to a Methanol Equivalent by $B(C_6F_5)_3$-Activated Alkaline Earth Catalysis. *Chem. Sci.* **2014**, *5*, 2826−2830. (d) Mukherjee, D.; Osseili, H.; Spaniol, T. P.; Okuda, J. Alkali Metal Hydridotriphenylborates $[(L)M][HBPh_3]$ (M = Li, Na, K): Chemoselective Catalysts for Carbonyl and CO_2 Hydroboration. *J. Am. Chem. Soc.* **2016**, *138*, 10790−10793. (e) Mukherjee, D.; Shirase, S.; Spaniol, T. P.; Mashima, K.; Okuda, J. Magnesium Hydridotriphenylborate $[Mg(thf)_6][HBPh_3]_2$: A Versatile Hydroboration Catalyst. *Chem. Commun.* **2016**, *52*, 13155−13158. (f) Mukherjee, D.; Wiegand, A.-K.; Spaniol, T. P.; Okuda, J. Zinc Hydridotriphenylborates Supported by a Neutral Macrocyclic Polyamine. *Dalton Trans.* **2017**, *46*, 6183−6186.
(9) Lu, Z.; Williams, T. J. Di(carbene)-Supported Nickel Systems for CO_2 Reduction Under Ambient Conditions. *ACS Catal.* **2016**, *6*, 6670−6673.
(10) $LiBH_4$, which is a more reactive borohydride than $NaBH_4$, can reduce CO_2 to $LiB(OCH_3)_4$ in the absence of a catalyst. For details, see: Burr, J. G., Jr.; Brown, W. G.; Heller, H. E. The Reduction of Carbon Dioxide to Formic Acid. *J. Am. Chem. Soc.* **1950**, *72*, 2560−2562.
(11) Heiden, Z. M.; Lathem, A. P. Establishing the Hydride Donor Abilities of Main Group Hydrides. *Organometallics* **2015**, *34*, 1818−1827.
(12) (a) Chong, C. C.; Kinjo, R. Catalytic Hydroboration of Carbonyl Derivatives, Imines, and Carbon Dioxide. *ACS Catal.* **2015**, *5*, 3238−3259. (b) Bontemps, S. Boron-Mediated Activation of Carbon Dioxide. *Coord. Chem. Rev.* **2016**, *308*, 117−130. (c) Wang, X.; Xia, C.; Wu, L. Homogeneous Carbon Dioxide Reduction with p-Block Element-Containing Reductants. *Green Chem.* **2018**, *20*, 5415−5426. (d) Zhang, J.; Chang, J.; Liu, T.; Cao, B.; Ding, Y.; Chen, X. Application of POCOP Pincer Nickel Complexes to the Catalytic Hydroboration of Carbon Dioxide. *Catalysts* **2018**, *8*, 508. (e) Kostera, S.; Peruzzini, M.; Gonsalvi, L. Recent Advances in Metal Catalyst Design for CO_2 Hydroboration to C1 Derivatives. *Catalysts* **2021**, *11*, 58. (f) Ma, N.; Xu, Q.; Zhang, G. Theoretical Insights on Boron Reducing Agent for the Reduction of Carbonyl Compounds. *Phys. Chem. Chem. Phys.* **2021**, *23*, 19111−19119.
(13) (a) Das Neves Gomes, C.; Blondiaux, E.; Thuéry, P.; Cantat, T. Metal-Free Reduction of CO_2 with Hydroboranes: Two Efficient Pathways at Play for the Reduction of CO_2 to Methanol. *Chem. − Eur. J.* **2014**, *20*, 7098−7106. (b) Légaré, M.-A.; Courtemanche, M.-A.; Fontaine, F.-G. Lewis Base Activation of Borane-Dimethylsulfide into Strongly Reducing Ion Pairs for the Transformation of Carbon Dioxide to Methoxyboranes. *Chem. Commun.* **2014**, *50*, 11362−11365.
(14) Wang, T.; Stephan, D. W. Phosphine Catalyzed Reduction of CO_2 with Boranes. *Chem. Commun.* **2014**, *50*, 7007−7010.
(15) (a) Yang, Y.; Xu, M.; Song, D. Organocatalysts with Carbon-Centered Activity for CO_2 Reduction with Boranes. *Chem. Commun.* **2015**, *51*, 11293−11296. (b) Janes, T.; Osten, K. M.; Pantaleo, A.; Yan, E.; Yang, Y.; Song, D. Insertion of CO_2 into the Carbon-Boron Bond of a Boronic Ester Ligand. *Chem. Commun.* **2016**, *52*, 4148−4151. (c) Sau, S. C.; Bhattacharjee, R.; Vardhanapu, P. K.; Vijaykumar, G.; Datta, A.; Mandal, S. K. Metal-Free Reduction of CO_2 to Methoxyborane under Ambient Conditions through Borondiformate Formation. *Angew. Chem., Int. Ed.* **2016**, *55*, 15147−15151. (d) Yang, Y.; Yan, L.; Xie, Q.; Liang, Q.; Song, D. Zwitterionic Indenylammonium with Carbon-Centred Reactivity Towards Reversible CO_2 Binding and Catalytic Reduction. *Org. Biomol. Chem.* **2017**, *15*, 2240−2245.
(16) (a) Courtemanche, M.-A.; Légaré, M.-A.; Maron, L.; Fontaine, F.-G. A Highly Active Phosphine-Borane Organocatalyst for the Reduction of CO_2 to Methanol Using Hydroboranes. *J. Am. Chem. Soc.* **2013**, *135*, 9326−9329. (b) Courtemanche, M.-A.; Larouche, J.; Légaré, M.-A.; Bi, W.; Maron, L.; Fontaine, F.-G. A Tris-(triphenylphosphine)aluminum Ambiphilic Precatalyst for the Reduction of Carbon Dioxide with Catecholborane. *Organometallics* **2013**, *32*, 6804−6811. (c) Wang, T.; Stephan, D. W. Carbene-9-BBN Ring Expansions as a Route to Intramolecular Frustrated Lewis Pairs for CO_2 Reduction. *Chem. − Eur. J.* **2014**, *20*, 3036−3039. (d) Courtemanche, M.-A.; Légaré, M.-A.; Maron, L.; Fontaine, F.-G. Reducing CO_2 to Methanol Using Frustrated Lewis Pairs: On the Mechanism of Phosphine-Borane-Mediated Hydroboration of CO_2. *J. Am. Chem. Soc.* **2014**, *136*, 10708−10717. (e) Declercq, R.; Bouhadir, G.; Bourissou, D.; Légaré, M.-A.; Courtemanche, M.-A.; Nahi, K. S.; Bouchard, N.; Fontaine, F.-G.; Maron, L. Hydroboration of Carbon Dioxide Using Ambiphilic Phosphine-Borane Catalysts: On the Role of the Formaldehyde Adduct. *ACS Catal.* **2015**, *5*, 2513−2520. (f) Von Wolff, N.; Lefèvre, G.; Berthet, J.-C.; Thuéry, P.; Cantat, T. Implications of CO_2 Activation by Frustrated Lewis Pairs in the Catalytic Hydroboration of CO_2: A View Using N/Si^+ Frustrated Lewis Pairs. *ACS Catal.* **2016**, *6*, 4526−4535. (g) Tlili, A.; Voituriez, A.; Marinetti, A.; Thuéry, P.; Cantat, T. Synergistic Effects in Ambiphilic Phosphino-Borane Catalysts for the Hydroboration of CO_2. *Chem. Commun.* **2016**, *52*, 7553−7555. (h) Ramos, A.; Antiñolo, A.; Carrillo-Hermosilla, F.; Fernández-Galán, R.; Rodríguez-Diéguez, A.; García-Vivó, D. Carbodiimides as Catalysts

https://doi.org/10.1021/acs.organomet.3c00126
Organometallics 2023, 42, 1525−1537

for the Reduction of CO_2 with Boranes. *Chem. Commun.* **2018**, *54*, 4700−4703.
(17) (a) Ho, S. Y.-F.; So, C.-W.; Saffon-Merceron, N.; Mézailles, N. Formation of a Zwitterionic Boronium Species from the Reaction of a Stable Carbenoid with Borane: CO_2 Reduction. *Chem. Commun.* **2015**, *51*, 2107−2110. (b) Lafage, M.; Pujol, A.; Saffon-Merceron, N.; Mézailles, N. BH_3 Activation by Phosphorus-Stabilized Geminal Dianions: Synthesis of Ambiphilic Organoborane, DFT Studies, and Catalytic CO_2 Reduction into Methanol Derivatives. *ACS Catal.* **2016**, *6*, 3030−3035. (c) Franz, D.; Jandl, C.; Stark, C.; Inoue, S. Catalytic CO_2 Reduction with Boron- and Aluminum Hydrides. *ChemCatChem* **2019**, *11*, 5275−5281.
(18) (a) Chia, C.-C.; Teo, Y.-C.; Cham, N.; Ho, S. Y.-F.; Ng, Z.-H.; Toh, H.-M.; Mézailles, N.; So, C.-W. Aluminum-Hydride-Catalyzed Hydroboration of Carbon Dioxide. *Inorg. Chem.* **2021**, *60*, 4569−4577. (b) Yan, B.; Dutta, S.; Ma, X.; Ni, C.; Koley, D.; Yang, Z.; Roesky, H. W. Organoaluminum Hydrides Catalyzed Hydroboration of Carbonates, Esters, Carboxylic Acids, and Carbon Dioxide. *Dalton Trans.* **2022**, *51*, 6756−6765.
(19) (a) Abdalla, J. A. B.; Riddlestone, I. M.; Tirfoin, R.; Aldridge, S. Cooperative Bond Activation and Catalytic Reduction of Carbon Dioxide at a Group 13 Metal Center. *Angew. Chem., Int. Ed.* **2015**, *54*, 5098−5102. (b) Liu, L.; Lo, S.-K.; Smith, C.; Goicoechea, J. M. Pincer-Supported Gallium Complexes for the Catalytic Hydroboration of Aldehydes, Ketones and Carbon Dioxide. *Chem. − Eur. J.* **2021**, *27*, 17379−17385.
(20) Hadlington, T. J.; Kefalidis, C. E.; Maron, L.; Jones, C. Efficient Reduction of Carbon Dioxide to Methanol Equivalents Catalyzed by Two-Coordinate Amido−Germanium(II) and −Tin(II) Hydride Complexes. *ACS Catal.* **2017**, *7*, 1853−1859.
(21) Pal, R.; Groy, T. L.; Trovitch, R. J. Conversion of Carbon Dioxide to Methanol Using a C−H Activated Bis(imino)pyridine Molybdenum Hydroboration Catalyst. *Inorg. Chem.* **2015**, *54*, 7506−7515.
(22) (a) Erken, C.; Kaithal, A.; Sen, S.; Weyhermüller, T.; Hölscher, M.; Werlé, C.; Leitner, W. Manganese-Catalyzed Hydroboration of Carbon Dioxide and Other Challenging Carbonyl Groups. *Nat. Commun.* **2018**, *9*, 4521. (b) Kostera, S.; Peruzzini, M.; Kirchner, K.; Gonsalvi, L. Mild and Selective Carbon Dioxide Hydroboration to Methoxyboranes Catalyzed by Mn(I) PNP Pincer Complexes. *ChemCatChem* **2020**, *12*, 4625−4631.
(23) Aloisi, A.; Berthet, J.-C.; Genre, C.; Thuéry, P.; Cantat, T. Complexes of the Tripodal Phosphine Ligands $PhSi(XPPh_2)_3$ (X = CH_2, O): Synthesis, Structure and Catalytic Activity in the Hydroboration of CO_2. *Dalton Trans.* **2016**, *45*, 14774−14788.
(24) (a) Bontemps, S.; Vendier, L.; Sabo-Etienne, S. Borane-Mediated Carbon Dioxide Reduction at Ruthenium: Formation of C_1 and C_2 Compounds. *Angew. Chem., Int. Ed.* **2012**, *51*, 1671−1674. (b) Sgro, M. J.; Stephan, D. W. Frustrated Lewis Pair Inspired Carbon Dioxide Reduction by a Ruthenium Tris(aminophosphine) Complex. *Angew. Chem., Int. Ed.* **2012**, *51*, 11343−11345. (c) Bontemps, S.; Sabo-Etienne, S. Trapping Formaldehyde in the Homogeneous Catalytic Reduction of Carbon Dioxide. *Angew. Chem., Int. Ed.* **2013**, *52*, 10253−10255. (d) Ng, C. K.; Wu, J.; Hor, T. S. A.; Luo, H.-K. A Binary Catalyst System of a Cationic Ru−CNC Pincer Complex with an Alkali Metal Salt for Selective Hydroboration of Carbon Dioxide. *Chem. Commun.* **2016**, *52*, 11842−11845.
(25) Tamang, S. R.; Findlater, M. Cobalt Catalysed Reduction of CO_2 *via* Hydroboration. *Dalton Trans.* **2018**, *47*, 8199−8203.
(26) Sánchez, P.; Hernández-Juárez, M.; Rendón, N.; López-Serrano, J.; Álvarez, E.; Paneque, M.; Suárez, A. Hydroboration of Carbon Dioxide with Catechol- and Pinacolborane Using an Ir−CNP* Pincer Complex. Water Influence on the Catalytic Activity. *Dalton Trans.* **2018**, *47*, 16766−16776.
(27) (a) Chakraborty, S.; Zhang, J.; Krause, J. A.; Guan, H. An Efficient Nickel Catalyst for the Reduction of Carbon Dioxide with a Borane. *J. Am. Chem. Soc.* **2010**, *132*, 8872−8873. (b) Huang, F.; Zhang, C.; Jiang, J.; Wang, Z.-X.; Guan, H. How Does the Nickel Pincer Complex Catalyze the Conversion of CO_2 to a Methanol Derivative? A Computational Mechanistic Study. *Inorg. Chem.* **2011**, *50*, 3816−3825. (c) Chakraborty, S.; Patel, Y. J.; Krause, J. A.; Guan, H. Catalytic Properties of Nickel Bis(phosphinite) Pincer Complexes in the Reduction of CO_2 to Methanol Derivatives. *Polyhedron* **2012**, *32*, 30−34. (d) Chakraborty, S.; Zhang, J.; Patel, Y. J.; Krause, J. A.; Guan, H. Pincer-Ligated Nickel Hydridoborate Complexes: the Dormant Species in Catalytic Reduction of Carbon Dioxide with Boranes. *Inorg. Chem.* **2013**, *52*, 37−47. (e) Suh, H.-W.; Guard, L. M.; Hazari, N. Synthesis and Reactivity of a Masked PSiP Pincer Supported Nickel Hydride. *Polyhedron* **2014**, *84*, 37−43. (f) Liu, T.; Meng, W.; Ma, Q.-Q.; Zhang, J.; Li, H.; Li, S.; Zhao, Q.; Chen, X. Hydroboration of CO_2 Catalyzed by Bis(phosphinite) Pincer Ligated Nickel Thiolate Complexes. *Dalton Trans.* **2017**, *46*, 4504−4509. (g) Wellala, N. P. N.; Dong, H. T.; Krause, J. A.; Guan, H. Janus POCOP Pincer Complexes of Nickel. *Organometallics* **2018**, *37*, 4031−4039. (h) Espinosa, M. R.; Charboneau, D. J.; Garcia de Oliveira, A.; Hazari, N. Controlling Selectivity in the Hydroboration of Carbon Dioxide to the Formic Acid, Formaldehyde, and Methanol Oxidation Levels. *ACS Catal.* **2019**, *9*, 301−314.
(28) (a) Suh, H.-W.; Guard, L. M.; Hazari, N. A Mechanistic Study of Allene Carboxylation with CO_2 Resulting in the Development of a Pd(II) Pincer Complex for the Catalytic Hydroboration of CO_2. *Chem. Sci.* **2014**, *5*, 3859−3872. (b) Ma, Q.-Q.; Liu, T.; Li, S.; Zhang, J.; Chen, X.; Guan, H. Highly Efficient Reduction of Carbon Dioxide with a Borane Catalyzed by Bis(phosphinite) Pincer Ligated Palladium Thiolate Complexes. *Chem. Commun.* **2016**, *52*, 14262−14265.
(29) Shintani, R.; Nozaki, K. Copper-Catalyzed Hydroboration of Carbon Dioxide. *Organometallics* **2013**, *32*, 2459−2462.
(30) (a) Wang, X.; Chang, K.; Xu, X. Hydroboration of Carbon Dioxide Enabled by Molecular Zinc Dihydrides. *Dalton Trans.* **2020**, *49*, 7324−7327. (b) He, W.; Liu, X.; Cui, D. Hydroboration of CO_2 Catalyzed by Heteroscorpionate Zwitterionic Zinc and Magnesium Hydride Complexes. *Dalton Trans.* **2022**, *51*, 4786−4789.
(31) Ma, N.; Tu, C.; Xu, Q.; Guo, W.; Zhang, J.; Zhang, G. Computational Study on the Mechanism of Hydroboration of CO_2 Catalysed by POCOP Pincer Nickel Thiolate Complexes: Concerted Catalysis and Hydride Transfer by a Shuttle. *Dalton Trans.* **2021**, *50*, 2903−2914.
(32) Ma, N.; Xu, Q.; Tu, C.; Guo, W.; Zhang, G. Ni Pincer Complex Catalytic Hydroboration of CO_2: a DFT Study on the Influence of Borane Reductants on Selective Reduction. *New J. Chem.* **2021**, *45*, 11275−11283.
(33) Suh, H.-W.; Schmeier, T. J.; Hazari, N.; Kemp, R. A.; Takase, M. K. Experimental and Computational Studies of the Reaction of Carbon Dioxide with Pincer-Supported Nickel and Palladium Hydrides. *Organometallics* **2012**, *31*, 8225−8236.
(34) For truncated PSiP-type hydride complexes, CO_2 insertion is kinetically more favorable with palladium but thermodynamically more favorable with nickel.
(35) Zhang, J.; Ding, Y.; Ma, Q.-Q.; Cao, B.; Chang, J.; Li, S.; Chen, X. Reactions of POCOP Pincer Palladium Benzylthiolate Complexes with BH_3•THF: Isolation and Characterization of Unstable POCOP-Pd(η^1-HBH_3) Complexes. *J. Organomet. Chem.* **2019**, *882*, 50−57.
(36) Adhikary, A.; Schwartz, J. R.; Meadows, L. M.; Krause, J. A.; Guan, H. Interaction of Alkynes with Palladium POCOP-Pincer Hydride Complexes and Its Unexpected Relation to Palladium-Catalyzed Hydrogenation of Alkynes. *Inorg. Chem. Front.* **2014**, *1*, 71−82.
(37) ^{t}Bu = *tert*-butyl, ^{i}Pr = isopropyl, ^{c}Pe = cyclopentyl.
(38) Johansson, R.; Wendt, O. F. Synthesis and Reactivity of (PCP) Palladium Hydroxy Carbonyl and Related Complexes toward CO_2 and Phenylacetylene. *Organometallics* **2007**, *26*, 2426−2430.
(39) In an attempt to fully dissolve 10 mg of **2a** in 0.5 mL of C_6D_6, the mixture (in a J. Young NMR tube) was gently heated, which resulted in ∼20% of **2a** being reverted back to **1a**.
(40) (a) Grove, D. M.; van Koten, G.; Ubbels, H. J. C.; Zoet, R.; Spek, A. L. Organonickel(II) Complexes of the Terdentate Monoanionic Ligand *o*,*o*′-Bis[(dimethylamino)methyl]phenyl (N-C-

https://doi.org/10.1021/acs.organomet.3c00126
Organometallics 2023, 42, 1525−1537

N). Syntheses and the X-ray Crystal Structure of the Stable Nickel(II) Formate [Ni(N-C-N)O_2CH]. *Organometallics* **1984**, *3*, 1003−1009. (b) Huang, D.; Holm, R. H. Reactions of the Terminal Ni^{II}−OH Group in Substitution and Electrophilic Reactions with Carbon Dioxide and Other Substrates: Structural Definition of Binding Modes in an Intramolecular Ni^{II}···Fe^{II} Bridged Site. *J. Am. Chem. Soc.* **2010**, *132*, 4693−4701. (c) Schmeier, T. J.; Hazari, N.; Incarvito, C. D.; Raskatov, J. A. Exploring the Reactions of CO_2 with PCP Supported Nickel Complexes. *Chem. Commun.* **2011**, *47*, 1824−1826. (d) Yoo, C.; Kim, J.; Lee, Y. Synthesis and Reactivity of Nickel(II) Hydroxycarbonyl Species, NiCOOH-κC. *Organometallics* **2013**, *32*, 7195−7203. (e) Jonasson, K. J.; Wendt, O. F. Synthesis and Characterization of a Family of POCOP Pincer Complexes with Nickel: Reactivity Towards CO_2 and Phenylacetylene. *Chem. − Eur. J.* **2014**, *20*, 11894−11902. (f) Murugesan, S.; Stöger, B.; Weil, M.; Veiros, L. F.; Kirchner, K. Synthesis, Structure, and Reactivity of Co(II) and Ni(II) PCP Pincer Borohydride Complexes. *Organometallics* **2015**, *34*, 1364−1372. (g) Kreye, M.; Freytag, M.; Jones, P. G.; Williard, P. G.; Bernskoetter, W. H.; Walter, M. D. Homolytic H_2 Cleavage by a Mercury-Bridged Ni(I) Pincer Complex [{(PNP)-Ni}$_2${μ-Hg}]. *Chem. Commun.* **2015**, *51*, 2946−2949.

(41) On the basis of the chemical shift value, the formation of the previously reported palladium borohydride complex {2,6-(^{t}Bu_2PO)$_2$$C_6H_3$}Pd($BH_4$) (δ 200.2, in C_6D_6) can be ruled out. For details, see ref 35.

(42) Zhang, J.; Medley, C. M.; Krause, J. A.; Guan, H. Mechanistic Insights into C−S Cross-Coupling Reactions Catalyzed by Nickel Bis(phosphinite) Pincer Complexes. *Organometallics* **2010**, *29*, 6393−6401.

(43) Petit, E.; Salles, F.; Alligier, D.; Demirci, U. B. Hydrolysis of the Borohydride Anion BH_4^-: A ^{11}B NMR Study Showing the Formation of Short-Living Reaction Intermediates Including BH_3OH^-. *Molecules* **2022**, *27*, 1975.

(44) Westcott, S. A.; Blom, H. P.; Marder, T. B.; Baker, R. T.; Calabrese, J. C. Nucleophile Promoted Degradation of Catecholborane: Consequences for Transition Metal-Catalyzed Hydroborations. *Inorg. Chem.* **1993**, *32*, 2175−2182.

(45) (a) Kanas, D. A.; Geier, S. J.; Vogels, C. M.; Decken, A.; Westcott, S. A. Synthesis, Characterization, and Reactivity of Rhodium(I) Acetylacetonato Complexes Containing Pyridinecarboxaldimine Ligands. *Inorg. Chem.* **2008**, *47*, 8727−8735. (b) Lee, G. M.; Vogels, C. M.; Decken, A.; Westcott, S. A. Iridium Phosphane Complexes Containing Arylspiroboronate Esters for the Hydroboration of Alkenes. *Eur. J. Inorg. Chem.* **2011**, 2433−2438. (c) Widera, A.; Kaifer, E.; Wadepohl, H.; Himmel, H.-J. On the Dual Reactivity of a Nucleophilic Dihydrido-Diborane: Reaction at the B−B Bond and/or the B−H Bond. *Chem. − Eur. J.* **2018**, *24*, 1209−1216. (d) Drescher, W.; Kleeberg, C. Terminal versus Bridging Boryl Coordination in N-Heterocyclic Carbene Copper(I) Boryl Complexes: Syntheses, Structures, and Dynamic Behavior. *Inorg. Chem.* **2019**, *58*, 8215−8229. (e) Kundu, G.; Dixit, R.; Tothadi, S.; Vanka, K.; Sen, S. S. Versatile Chemistry of Six-Membered NHC with Boranes: Bromination at sp^3 Borane, Activation of the B−H Bond of HBpin, and Ring Expansion of NHC. *Dalton Trans.* **2022**, *51*, 14452−14457.

(46) (a) Dai, C.; Robins, E. G.; Scott, A. J.; Clegg, W.; Yufit, D. S.; Howard, J. A. K.; Marder, T. B. Rhodium Catalysed Diboration of Unstrained Internal Alkenes and a New and General Route to Zwitterionic [L_2Rh(η^6-catBcat)] (cat = 1,2-$O_2C_6H_4$) Complexes. *Chem. Commun.* **1998**, 1983−1984. (b) Westcott, S. A.; Marder, T. B.; Baker, R. T.; Harlow, R. L.; Calabrese, J. C.; Lam, K. C.; Lin, Z. Reactions of Hydroborating Reagents with Phosphinorhodium Hydride Complexes: Molecular Structures of a Rh_2B_3 Metallaborane Cluster, an L_2Rh(η^2-H_2BR_2) Complex and a Mixed Valence Rh Dimer Containing a Semi-bridging Bcat (cat = 1,2-$O_2C_6H_4$) Group. *Polyhedron* **2004**, *23*, 2665−2677. (c) Geier, S. J.; Chapman, E. E.; McIsaac, D. I.; Vogels, C. M.; Decken, A.; Westcott, S. A. Bulky Rhodium Diimine Complexes for the Catalyzed Borylation of Vinylarenes. *Inorg. Chem. Commun.* **2006**, *9*, 788−791. (d) Melanson, J. A.; Vogels, C. M.; Decken, A.; Westcott, S. A. Catalytic Hydroboration of Vinylarenes Using a Zwitterionic Arylspiroboronate Ester Iridium Complex. *Inorg. Chem. Commun.* **2010**, *13*, 1396−1398.

(47) (a) He, X.; Hartwig, J. F. True Metal-Catalyzed Hydroboration with Titanium. *J. Am. Chem. Soc.* **1996**, *118*, 1696−1702. (b) Manßen, M.; Meyer, M.-F.; Schmidtmann, M.; Beckhaus, R. Direct Access to Terminal Titanocene Hydrazides via Bis(η^5:η^1-pentafulvene)titanium Complexes and 1,1-Diphenylhydrazine. *Organometallics* **2018**, *37*, 4515−4520.

(48) The κ^1-coordination mode of $[B(cat)_2]^-$ has been found in Li and Ag compounds. For details, see: (a) Downard, A.; Nieuwenhuyzen, M.; Seddon, K. R.; van den Berg, J.-A.; Schmidt, M. A.; Vaughan, J. F. S.; Welz-Biermann, U. Structural Features of Lithium Organoborates. *Cryst. Growth Des.* **2002**, *2*, 111−119. (b) Arévalo, R.; Vogels, C. M.; MacNeil, G. A.; Riera, L.; Pérez, J.; Westcott, S. A. Rhenium-Catalysed Hydroboration of Aldehydes and Aldimines. *Dalton Trans.* **2017**, *46*, 7750−7757.

(49) Knizek, J.; Nöth, H. Tris(2,6-diisopropylphenolato)titanium-(IV) Dihydridodiorganylborates: Synthesis and Structures. *Eur. J. Inorg. Chem.* **2011**, *2011*, 1888−1900.

(50) Männig, D.; Nöth, H. Contributions to the Chemistry of Boron. Part 160. A Convenient Synthesis of Catecholatoborane and Diborane. *J. Chem. Soc., Dalton Trans.* **1985**, 1689−1692.

(51) (a) Waltz, K. M.; Hartwig, J. F. Functionalization of Alkanes by Isolated Transition Metal Boryl Complexes. *J. Am. Chem. Soc.* **2000**, *122*, 11358−11369. (b) Adhikari, D.; Huffman, J. C.; Mindiola, D. J. Structural Elucidation of a Nickel Boryl Complex. A Recyclable Borylation Ni(II) Reagent of Bromobenzene. *Chem. Commun.* **2007**, 4489−4491.

(52) Zhu, Y.; Chen, C.-H.; Fafard, C. M.; Foxman, B. M.; Ozerov, O. V. Net Heterolytic Cleavage of B−H and B−B Bonds Across the N−Pd Bond in a Cationic (PNP)Pd Fragment. *Inorg. Chem.* **2011**, *50*, 7980−7987.

(53) Wilson, G. L. O.; Abraha, M.; Krause, J. A.; Guan, H. Reactions of Phenylacetylene with Nickel POCOP-Pincer Hydride Complexes Resulting in Different Outcomes from Their Palladium Analogues. *Dalton Trans.* **2015**, *44*, 12128−12136.

(54) An *N*-heterocyclic carbene (NHC) supported copper boryl complex has been shown to react with CO_2 or an aldehyde to form an (NHC)Cu−OR species. For details, see: (a) Laitar, D. S.; Müller, P.; Sadighi, J. P. Efficient Homogeneous Catalysis in the Reduction of CO_2 to CO. *J. Am. Chem. Soc.* **2005**, *127*, 17196−17197. (b) Laitar, D. S.; Tsui, E. Y.; Sadighi, J. P. Catalytic Diboration of Aldehydes via Insertion into the Copper-Boron Bond. *J. Am. Chem. Soc.* **2006**, *128*, 11036−11037.

(55) Heimann, J. E.; Bernskoetter, W. H.; Hazari, N.; Mayer, J. M. Acceleration of CO_2 Insertion into Metal Hydrides: Ligand, Lewis Acid, and Solvent Effects on Reaction Kinetics. *Chem. Sci.* **2018**, *9*, 6629−6638.

https://doi.org/10.1021/acs.organomet.3c00126
Organometallics 2023, 42, 1525−1537